J Sci Comput (2016) 68:1241–1266
DOI 10.1007/s10915-016-0177-x

Semi-Discrete Energy-Stable Schemes for a Tensor-Based Hydrodynamic Model of Nematic Liquid Crystal Flows

Jia Zhao[1] · **Qi Wang**[1,2,3]

Received: 29 July 2015 / Revised: 23 January 2016 / Accepted: 27 January 2016 /
Published online: 3 February 2016

Abstract In this paper, we develop a first-order and a second-order coupled energy stable numerical scheme respectively for a Q-tensor based hydrodynamic model of nematic liquid crystal flows. We then extend the first order coupled scheme to a decoupled scheme and show that it is energy stable as well. The fully coupled schemes are implemented in 2-dimensional space and time, with which we study defect dynamics in flows of nematic liquid crystals in a channel. The numerical schemes are shown to be efficient in solving the Q-tensor based liquid crystal model. The methodology developed here also provides a paradigm for developing energy-stable schemes for more general hydrodynamic models of complex fluids which obey an energy dissipation law.

Keywords Liquid crystals · Energy stable scheme · Finite difference · Hydrodynamics

1 Background

Nematic liquid crystals are complex fluids that exhibit an orientational order on average in their molecular orientation, but do not normally possess any positional order. Like other complex fluids, their rheological properties are primarily dominated by mesoscopic structures and dynamics. The most popular mathematical model for flows of low molecular weight nematic liquid crystals is the celebrated Ericksen–Leslie model [13], in which the average molecular orientation is described by a unit vector **p**, known as the director, and the distortional elasticity is described by the Oseen–Frank elastic energy. This theory is apolar in that it does

✉ Qi Wang
qwang@math.sc.edu

Jia Zhao
zhao62@math.sc.edu

1 Department of Mathematics, Interdisciplinary Mathematics Institute and NanoCenter at USC, University of South Carolina, Columbia, SC 29208, USA

2 Beijing Computational Science Research Center, Beijing 100193, China

3 School of Mathematics, Nankai University, Tianjin 300071, China

not differentiate the orientation between $\mathbf{p}$ and $-\mathbf{p}$. It describes uniaxial symmetry in all flow geometries including the shear flow and at defects, neglecting any potential biaxiality. However, in shear flows, orientational symmetry can readily be broken by the flow, leading to truly biaxial symmetry in nematic liquid crystals. In this case, the Ericksen–Leslie theory fails to capture this important broken symmetry. In fact, it has been show that the director model is in fact an asymptotic limit of a more general tensor model for liquid crystals [28].

An alternative to the director theory is to use the Q-tensor, a second order tensor of trace zero, which can be traced back to the deviatoric part of the second moment of a probability distribution function for the nematic liquid crystal system. The reflective symmetry of the system as well as biaxiality are naturally built in the tensor-based theories. Therefore, for flows of nematic liquid crystal polymers, a Q-tensor based hydrodynamic model of liquid crystals is more appropriate [1,8,9,25,28].

In the Q-tensor based Landau–de Gennes theory, the average orientation of nematic liquid crystals is described using $\mathbf{Q}$ [28]. We denote

$$\Lambda = \left\{ \mathbf{Q} \in \mathbb{R}^{3\times 3}, \quad tr(\mathbf{Q}) = 0, \quad \mathbf{Q} = \mathbf{Q}^T \right\}. \tag{1.1}$$

A nematic liquid crystal is said to be (i) isotropic when $\mathbf{Q} = 0$; (ii) uniaxial when $\mathbf{Q}$ has two equal non-zero eigenvalues:

$$\mathbf{Q} = s_1 \left(\mathbf{n} \otimes \mathbf{n} - \frac{1}{3}\mathbf{I} \right), \quad s_1 \in \mathbb{R}\backslash\{0\}, \mathbf{n} \in \mathbb{S}^2; \tag{1.2}$$

and biaxial when $\mathbf{Q}$ has three distinct eigenvalues:

$$\mathbf{Q} = s_1 \left(\mathbf{n} \times \mathbf{n} - \frac{1}{3}\mathbf{I} \right) + s_2 \left(\mathbf{m} \times \mathbf{m} - \frac{1}{3}\mathbf{I} \right), \quad s_1, s_2 \in \mathbb{R}\backslash\{0\}, \quad \mathbf{n}, \mathbf{m} \in \mathbb{S}^2, \mathbf{n} \perp \mathbf{m}. \tag{1.3}$$

Here the order parameters: s_1, s_2 are actually confined in a triangular region enclosing the origin [27]. They are linear combinations of eigenvalues of $\mathbf{Q}$. In nontrivial flows of nematic liquid crystals, all three phases may show up.

Now, we consider nematic liquid crystals in a smooth domain $\Omega \subset \mathbb{R}^3$. The total free energy F is given as follows:

$$F = \int_\Omega \left[\frac{K}{2} |\nabla \mathbf{Q}|^2 + g(\mathbf{Q}) \right] d\mathbf{x}, \tag{1.4}$$

with K the distortional elastic constant and the second term $g(\mathbf{Q})$ is the bulk free energy term. Although more general distortional elastic terms can be included, for the sake of simplicity, we stick to the one constant case in this paper [14]. We use the simplified Landau–de Gennes bulk free energy [4]

$$g(\mathbf{Q}) = \frac{a_1}{2} tr(\mathbf{Q}^2) + \frac{a_2}{3} tr(\mathbf{Q}^3) + \frac{a_3}{4} \left(tr(\mathbf{Q}^2) \right)^2, \tag{1.5}$$

where $a_{1,2,3}$ are model parameters for the bulk energy. For thermotropic liquid crystals, $a_1 \sim (T - T_0)$, T_0 is the phase transition temperature, and T the temperature of the liquid crystal, which controls the phase transition from the isotropic phase to the nematic phase. I.e. when $T_0 < T$, the equilibrium state is isotropic; when $T_0 > T$, it is nematic. For lyotropic liquid crystals, $a_1 = \alpha(1 - N/3), a_2 = -\alpha N, a_3 = \alpha N$, where N is the dimensionless concentration and α is a scaling parameter [6,28]. When, $0 \leq N < 3$, the system is in isotropic phase while it is in nematic phase when $N > 3$. There could also be an intermediate interval in N where both phases can coexist [27].

We denote the rate of strain tensor $\mathbf{D}$ and the vorticity tensor $\mathbf{W}$ as follows

$$\mathbf{D} = \frac{1}{2}\left(\nabla\mathbf{u} + \nabla\mathbf{u}^T\right), \quad \mathbf{W} = \frac{1}{2}\left(\nabla\mathbf{u} - \nabla\mathbf{u}^T\right), \tag{1.6}$$

with $(\nabla\mathbf{u})_{ij} = \partial_j \mathbf{u}_i$. The nondimensionalizsed Q-tensor model of nematic liquid crystals is summarized as follows [1,28,34]

$$\begin{cases} \mathbf{u}_t + \mathbf{u}\cdot\nabla\mathbf{u} = -\nabla p' + \eta\nabla^2\mathbf{u} + \nabla\cdot\sigma'(\mathbf{Q},\mathbf{H}) - \mathbf{H}\nabla\mathbf{Q}, \\ \nabla\cdot\mathbf{u} = 0, \\ \mathbf{Q}_t + \mathbf{u}\cdot\nabla\mathbf{Q} - S(\nabla\mathbf{u},\mathbf{Q}) = M_1\mathbf{H}, \end{cases} \tag{1.7}$$

where p' is the hydrostatic pressure, σ' is the elastic stress, $\mathbf{H}$ is the molecular field, $1/M_1$ is the relaxation time, $S(\nabla\mathbf{u},\mathbf{Q})$ is defined by

$$S(\nabla\mathbf{u},\mathbf{Q}) = \mathbf{W}\cdot\mathbf{Q} - \mathbf{Q}\cdot\mathbf{W} + a(\mathbf{Q}\cdot\mathbf{D} + \mathbf{D}\cdot\mathbf{Q}) + \tfrac{2a}{3}\mathbf{D} - 2a(\mathbf{D}:\mathbf{Q})\left(\mathbf{Q} + \tfrac{1}{3}\mathbf{I}\right), \tag{1.8}$$

a is a geometric parameter of the nematic liquid crystal molecule, confined between -1 and 1 [28]. Here the molecular field $\mathbf{H}$ is given by

$$\begin{aligned} \mathbf{H} &= -\left(\frac{\delta F}{\delta\mathbf{Q}} - \frac{1}{3}tr\left(\frac{\delta F}{\delta\mathbf{Q}}\right)\mathbf{I}\right) \\ &= K\nabla^2\mathbf{Q} - \left(a_1\mathbf{Q} - a_2\left(\mathbf{Q}^2 - \frac{1}{3}tr(\mathbf{Q}^2)\mathbf{I}\right) + a_3 tr(\mathbf{Q}^2)\mathbf{Q}\right), \end{aligned} \tag{1.9}$$

and the elastic stress σ' is given by

$$\sigma'(\mathbf{Q},\mathbf{H}) = (\mathbf{Q}\cdot\mathbf{H} - \mathbf{H}\cdot\mathbf{Q}) - a(\mathbf{H}\cdot\mathbf{Q} + \mathbf{Q}\cdot\mathbf{H}) - \frac{2a}{3}\mathbf{H} + 2a(\mathbf{Q}:\mathbf{H})\left(\mathbf{Q} + \frac{1}{3}\mathbf{I}\right). \tag{1.10}$$

This model has been used in studying liquid crystals especially flows of liquid crystal polymers extensively [4,5,16,22,28,32]. Despite that the model has been solved numerically repeatedly, no numerical analysis result has been established. There are some existing analytic work in literature on solution existence and regularity. In [10], the author showed the existence and uniqueness of a local-in-time weak solution with weak regularity for the time derivative of the velocity and the tensor variable ($\mathbf{u}$, $\mathbf{Q}$). In [7], the authors showed regularity criteria for local strong solutions. In [17], the authors proved the existence of global weak solutions in dimensions two and three in the entire space. In [11], the author considered the existence and uniqueness of weak solutions in a bounded three-dimensional domain under a homogeneous Dirichlet boundary condition for $\mathbf{u}$ and either a non-homogeneous Dirichlet or a homogeneous Neumann boundary condition for tensor $\mathbf{Q}$. Numerically, a few authors have designed numerical schemes to solve the equations. For instance, in [5], Yeomann et al. used the Lattice Boltzmann method to solve the model to study structures in nematic liquid crystals; in [15], the author presented numerical schemes for minimizing Landau–de Gennes energy based on a finite element discretization without hydrodynamics. There are several extensions of this model to study two phase fluid flows [23] and active liquid crystals recently [2]. However, no stability analysis has been established for the numerical schemes developed so far.

In fact, it can be shown that the Q-tensor nematic liquid crystal model (1.7) obeys an energy dissipation law, which will be presented in details in the next section. This indicates that the model can be derived using the generalized Onsager principle [33]. Naturally, one would like to design numerical schemes that approximate the continuum model and in the

meantime obey consistent discrete energy dissipation laws, which would be a good indication of a fine approximation to the continuum dissipative system. This type of numerical schemes is known as the energy stable scheme. However, to our best knowledge, such a numerical scheme for the Q-tensor hydrodynamic model of liquid crystals (1.7) has not been developed so far.

In this paper, we will develop several energy stable numerical schemes for this nematic liquid crystal model (1.7), based on a stabilization technique [20,30], the convex splitting strategy [19,26] and decoupling methods [3,21]. We will only discretize the scheme in time. For the spatial discretization, we can readily develop a second order finite difference discretization to retain the discrete energy in discrete norms under appropriate boundary conditions. For finite element and spectral methods, energy preserving discretization perhaps can be established as well, which will not be pursued in this paper. Thus, the numerical schemes can be validated for a broad spectrum of spatial-discretization strategies so long as the spatial discretization renders a faithful approximation to the total energy in the continuous system. The numerical schemes that we will develop in this study will address the following numerical issues directly:

- the coupling of the velocity and pressure through the incompressible condition;
- the stiffness in the tensor equation associated with nonlinear bulk terms $g(\mathbf{Q})$ (an explicit treatment of $g(\mathbf{Q})$ will lead to instability);
- the nonlinear coupling between the momentum transport and the tensor field equation.

The rest of the paper is organized as follows. In Sect. 2, we briefly derive the energy dissipation law of the nematic liquid crystal model (1.7). In Sect. 3, we present several semi-discrete numerical schemes for the model and prove their energy stability. Fully discretized schemes of course warrant thorough numerical analyses to prove their stability and convergence, which will be deferred to a future study. In Sect. 4, we present several numerical case studies on mesh-refinement and defect dynamics of nematic liquid crystal channel flows. We then give a concluding remark in the last section.

2 Energy Dissipation in the Nematic Liquid Crystal System

In this section, we show that model (1.7) satisfies an energy dissipation law. In order to simplify our proof, we rewrite the hydrostatic pressure p and elastic stress σ as

$$p = p' + \frac{2a}{3}(\mathbf{Q} : \mathbf{H}), \tag{2.1}$$

$$\sigma(\mathbf{Q}, \mathbf{H}) = \sigma'(\mathbf{Q}, \mathbf{H}) - \frac{2a}{3}(\mathbf{Q} : \mathbf{H})\mathbf{I}. \tag{2.2}$$

Then, the model is rewritten into

$$\begin{cases} \mathbf{u}_t + \mathbf{u} \cdot \nabla \mathbf{u} = -\nabla p + \eta \nabla^2 \mathbf{u} + \nabla \cdot \sigma(\mathbf{Q}, \mathbf{H}) - \mathbf{H} \nabla \mathbf{Q}, \\ \nabla \cdot \mathbf{u} = 0, \\ \mathbf{Q}_t + \mathbf{u} \cdot \nabla \mathbf{Q} - S(\nabla \mathbf{u}, \mathbf{Q}) = M_1 \mathbf{H}, \end{cases} \tag{2.3}$$

with

$$S(\nabla \mathbf{u}, \mathbf{Q}) = \mathbf{W}\cdot\mathbf{Q} - \mathbf{Q}\cdot\mathbf{W} + a(\mathbf{Q}\cdot\mathbf{D} + \mathbf{D}\cdot\mathbf{Q}) + \frac{2a}{3}\mathbf{D} - 2a(\mathbf{D}:\mathbf{Q})\left(\mathbf{Q} + \frac{1}{3}\mathbf{I}\right), \tag{2.4}$$

$$\sigma(\mathbf{Q}, \mathbf{H}) = (\mathbf{Q}\cdot\mathbf{H} - \mathbf{H}\cdot\mathbf{Q}) - a(\mathbf{H}\cdot\mathbf{Q} + \mathbf{Q}\cdot\mathbf{H}) - \frac{2a}{3}\mathbf{H} + 2a(\mathbf{Q}:\mathbf{H})\mathbf{Q}, \tag{2.5}$$

$$\mathbf{H} = K\nabla^2\mathbf{Q} - \left(a_1\mathbf{Q} - a_2(\mathbf{Q}^2 - \frac{1}{3}tr(\mathbf{Q}^2)\mathbf{I}) + a_3 tr(\mathbf{Q}^2)\mathbf{Q}\right). \tag{2.6}$$

In the following discussion, we will focus on deriving energy-stable numerical schemes on (2.3).

We consider a smooth domain Ω. For any two vector function $\mathbf{f} = (f_1, f_2, \ldots, f_d)$ and $\mathbf{g} = (g_1, g_2, \ldots, g_d)$, where $d \in N$, the inner product and norm are defined by

$$(\mathbf{f}, \mathbf{g}) = \sum_{i=1}^{d}\int_\Omega f_i g_i d\mathbf{x}, \quad \|\mathbf{f}\| = \sqrt{(\mathbf{f}, \mathbf{f})}. \tag{2.7}$$

First, we present the following lemmas.

Lemma 2.1 *The following identity holds for any vector function* $\mathbf{u}$*,*

$$((\mathbf{v}\cdot\nabla)\mathbf{u}, \mathbf{u}) = 0, \tag{2.8}$$

provided that $\mathbf{n}\cdot\mathbf{v}|_{\partial\Omega} = 0$*,* $\mathbf{v}$ *and* $\mathbf{u}$ *are sufficiently smooth and* $\nabla\cdot\mathbf{v} = 0$*, where* $\mathbf{n}$ *is the unit external normal of the boundary* $\partial\Omega$*.*

Lemma 2.2 *The following identity holds for any scalar function* p*,*

$$(\mathbf{v}, \nabla p) = 0, \tag{2.9}$$

provided that $\mathbf{n}\cdot\mathbf{v}|_{\partial\Omega} = 0$*,* $\mathbf{v}$ *is sufficiently smooth and* $\nabla\cdot\mathbf{v} = 0$*, where* $\mathbf{n}$ *is the unit external normal of the boundary.*

The proof of Lemma 2.1 and 2.2 are straight forward. Readers can refer to [24] for details.

Lemma 2.3 *Given a smooth domain* Ω*, if* $\mathbf{u} \in \mathbb{R}^3$ *with* $\mathbf{u}|_{\partial\Omega} = 0$*, and* $\mathbf{Q}, \mathbf{H} \in \Lambda$*, the following identity holds*

$$(\nabla\cdot\sigma(\mathbf{Q}, \mathbf{H}), \mathbf{u}) = (\mathbf{H}, S(\nabla\mathbf{u}, \mathbf{Q})), \tag{2.10}$$

where $\sigma(\mathbf{Q}, \mathbf{H})$ *is defined in* (2.5) *and* $S(\nabla\mathbf{u}, \mathbf{Q})$ *in* (2.4)*.*

Proof Recall from (2.4) and (2.5) that

$$S(\nabla\mathbf{u}, \mathbf{Q}) = (\mathbf{W}\cdot\mathbf{Q} - \mathbf{Q}\cdot\mathbf{W}) + a(\mathbf{D}\cdot\mathbf{Q} + \mathbf{Q}\cdot\mathbf{D}) + \frac{2a}{3}\mathbf{D} - 2a(\mathbf{Q}:\mathbf{D})\left(\mathbf{Q} + \frac{1}{3}\mathbf{I}\right),$$

$$\sigma(\mathbf{Q}, \mathbf{H}) = (\mathbf{Q}\cdot\mathbf{H} - \mathbf{H}\cdot\mathbf{Q}) - a(\mathbf{H}\cdot\mathbf{Q} + \mathbf{Q}\cdot\mathbf{H}) - \frac{2a}{3}\mathbf{H} + 2a(\mathbf{Q}:\mathbf{H})\mathbf{Q}. \tag{2.11}$$

For the left hand side, we have

$$\begin{aligned}(\nabla\cdot\sigma(\mathbf{Q}, \mathbf{H}), \mathbf{u}) &= (\nabla\cdot(\sigma\mathbf{u}), 1) - (\sigma, \nabla\mathbf{u}) \\ &= \left(-(\mathbf{Q}\cdot\mathbf{H} - \mathbf{H}\cdot\mathbf{Q}) + a(\mathbf{H}\cdot\mathbf{Q} + \mathbf{Q}\cdot\mathbf{H}) + \tfrac{2a}{3}\mathbf{H} + 2a(\mathbf{Q}:\mathbf{H})\mathbf{Q}, \nabla\mathbf{u}\right).\end{aligned} \tag{2.12}$$

provided $\mathbf{u}|_{\partial\Omega} = 0$.

For the right hand side, we have

$$\begin{aligned}&(\mathbf{H}, \quad S(\nabla\mathbf{u}, \mathbf{Q}))\\ &= \left(\mathbf{H}, \quad (\mathbf{W}\cdot\mathbf{Q} - \mathbf{Q}\cdot\mathbf{W}) + a(\mathbf{D}\cdot\mathbf{Q} + \mathbf{Q}\cdot\mathbf{D}) + \tfrac{2a}{3}\mathbf{D} - 2a(\mathbf{Q}:\mathbf{D})\left(\mathbf{Q} + \tfrac{1}{3}\mathbf{I}\right)\right).\end{aligned} \tag{2.13}$$

Notice the facts that

$$\begin{aligned}-(\mathbf{Q}\cdot\mathbf{H} - \mathbf{H}\cdot\mathbf{Q}, \nabla\mathbf{u}) &= (\mathbf{H}, \mathbf{W}\cdot\mathbf{Q} - \mathbf{Q}\cdot\mathbf{W}),\\ a(\mathbf{H}\cdot\mathbf{Q} + \mathbf{Q}\cdot\mathbf{H}, \nabla\mathbf{u}) &= a(\mathbf{H}, \mathbf{D}\cdot\mathbf{Q} + \mathbf{Q}\cdot\mathbf{D}),\\ 2a\,((\mathbf{Q}:\mathbf{H})\mathbf{Q}, \nabla\mathbf{u}) &= 2a\left(\mathbf{H}, (\mathbf{Q}:\mathbf{D})(\mathbf{Q} + \frac{1}{3}\mathbf{I})\right),\\ \frac{2a}{3}(\mathbf{H}, \nabla\mathbf{u}) &= \frac{2a}{3}(\mathbf{H}, \mathbf{D}).\end{aligned} \tag{2.14}$$

Adding the left hand side up, we obtain $(\nabla\cdot\sigma, \mathbf{u})$. Analogously, adding the right hand side, we have $(\mathbf{H}, S(\nabla\mathbf{u}, \mathbf{Q}))$.

So, given $\mathbf{u}|_{\partial\Omega} = 0$, we arrive at

$$(\nabla\cdot\sigma(\mathbf{Q}, \mathbf{H}), \mathbf{u}) = (\mathbf{H}, S(\nabla\mathbf{u}, \mathbf{Q}))\,. \tag{2.15}$$

□

Lemma 2.4 *Recall the Landau–de Gennes bulk potential in (1.5). We can rewrite it as*

$$f(\mathbf{Q}) = f_1(\mathbf{Q}) - f_2(\mathbf{Q}), \tag{2.16}$$

where

$$\begin{aligned}f_1(\mathbf{Q}) &= \frac{b_1}{2}tr(\mathbf{Q}^2) + \frac{a_2}{3}tr(\mathbf{Q}^3) + \frac{b_3}{4}(tr(\mathbf{Q}^2))^2,\\ f_2(\mathbf{Q}) &= \frac{b_1 - a_1}{2}tr(\mathbf{Q}^2) + \frac{b_3 - a_3}{4}(tr(\mathbf{Q}^2))^2.\end{aligned} \tag{2.17}$$

If $b_1 > \max(|a_2|, |a_1|)$ and $b_3 > |a_2|$, $f_1(\mathbf{Q})$ and $f_2(\mathbf{Q})$ are convex functions.

Proof We only need to prove the Hessian matrix of f_1 and f_2 are positive-definite. For notation simplicity, we use the index notations, i.e. $(\mathbf{Q})_{ij} = Q_{ij}$, and we use the notational convention of Einstein summation.

For this bulk potential

$$f_1(\mathbf{Q}) = \frac{b_1}{2}tr(\mathbf{Q}^2) + \frac{a_2}{3}tr(\mathbf{Q}^3) + \frac{b_3}{4}(tr(\mathbf{Q}^2))^2, \tag{2.18}$$

we can get

$$\frac{\partial f_1}{\partial Q_{ij}} = b_1 Q_{ij} + a_2 Q_{ik}Q_{kj} + b_3(Q_{ks}Q_{ks})Q_{ij}. \tag{2.19}$$

And the Hessian matrix could be calculated as

$$\begin{aligned}\mathcal{H}_1 &= \frac{\partial^2 f_1}{\partial Q_{ij}\partial Q_{mn}}\\ &= b_1\delta_{im}\delta_{jn} + a_2\left(\delta_{im}\delta_{kn}Q_{kj} + \delta_{km}\delta_{jn}Q_{ik}\right) + b_3(Q_{ks}Q_{ks})\delta_{im}\delta_{jn} + 2b_3\delta_{km}\delta_{sn}Q_{ks}Q_{ij}\\ &= b_1\delta_{im}\delta_{jn} + a_2\left(\delta_{im}Q_{nj} + \delta_{jn}Q_{im}\right) + b_3(Q_{ks}Q_{ks})\delta_{im}\delta_{jn} + 2b_3Q_{mn}Q_{ij}\end{aligned} \tag{2.20}$$

If we multiply left side of $\mathcal{H}_1$ by x_{ij}, right side of $\mathcal{H}_1$ by x_{mn}, we obtain,

$$\begin{aligned} x_{ij}\mathcal{H}_1 x_{mn} &= b_1 x_{mn}x_{mn} + 2a_2 x_{mj}Q_{nj}x_{mn} + b_3(Q_{ks}Q_{ks})x_{mn}x_{mn} + 2b_3(x_{mn}Q_{mn})^2 \\ &\geq b_1 x_{mn}x_{mn} - 2|a_2|\sqrt{Q_{ks}Q_{ks}}x_{mn}x_{mn} + b_3(Q_{ks}Q_{ks})x_{mn}x_{mn} \\ &\geq |a_2|(\sqrt{Q_{ks}Q_{ks}} - 1)^2 x_{mn}x_{mn} \\ &\geq 0, \end{aligned} \tag{2.21}$$

since $b_1 > max(|a_2|, |a_1|)$ and $b_3 > |a_2|$. Therefore, $f_1(\mathbf{Q})$ is a convex function. In the same manner, it is easy to show $f_2(\mathbf{Q})$ is also a convex function. □

The energy dissipation law of model (2.3) is summarized in the following theorem.

Theorem 2.1 *We denote the total energy as* $\mathscr{E}$

$$\mathscr{E} = \int_\Omega \left[\frac{1}{2}\mathbf{u}^2 + f\right] d\mathbf{x}, \tag{2.22}$$

where the first term $\frac{1}{2}\mathbf{u}^2$ *is the kinetic energy density and* f *is the free energy density given by*

$$f = \frac{K}{2}|\nabla \mathbf{Q}|^2 + \frac{a_1}{2}tr(\mathbf{Q}^2) + \frac{a_2}{2}tr(\mathbf{Q}^3) + \frac{a_3}{4}(tr(\mathbf{Q}^2))^2. \tag{2.23}$$

The energy dissipation rate (or negative of the entropy production rate) of system (2.3) *is given by*

$$\frac{d\mathscr{E}}{dt} = -\int_\Omega \left[\eta|\nabla \mathbf{u}|^2 + M_1|\mathbf{H}|^2\right] d\mathbf{x}. \tag{2.24}$$

Proof The time rate of change for the total energy is calculated as follows:

$$\begin{aligned} \frac{d\mathscr{E}}{dt} &= \frac{d}{dt}\int_\Omega \left[\frac{1}{2}\mathbf{u}^2 + f\right] d\mathbf{x} \\ &= \int_\Omega \left(\mathbf{u}\cdot\partial_t\mathbf{u} + \frac{\delta F}{\delta \mathbf{Q}}\partial_t\mathbf{Q}\right) d\mathbf{x}. \end{aligned} \tag{2.25}$$

Notice from (2.3) that

$$\begin{aligned} \mathbf{u}_t &= -\mathbf{u}\cdot\nabla\mathbf{u} - \nabla p + \eta\nabla^2\mathbf{u} + \nabla\cdot\sigma(\mathbf{Q},\mathbf{H}) - \mathbf{H}\nabla\mathbf{Q}, \\ \mathbf{Q}_t &= -\mathbf{u}\cdot\nabla\mathbf{Q} + S(\nabla\mathbf{u},\mathbf{Q}) + M_1\mathbf{H}. \end{aligned} \tag{2.26}$$

By substituting (2.26) into (2.25), we obtain

$$\begin{aligned} \frac{d\mathscr{E}}{dt} = \int_\Omega \big[\mathbf{u}\cdot\big(-\mathbf{u}\cdot\nabla\mathbf{u} - \nabla p + \eta\nabla^2\mathbf{u} + \nabla\cdot\sigma(\mathbf{Q},\mathbf{H}) - \mathbf{H}\nabla\mathbf{Q}\big) + \\ -\mathbf{H}\cdot(-\mathbf{u}\cdot\nabla\mathbf{Q} + S(\nabla\mathbf{u},\mathbf{Q}) + M_1\mathbf{H})\big] d\mathbf{x}. \end{aligned} \tag{2.27}$$

Using Lemmas 2.1, 2.2 and 2.3, we have respectively

$$\int_\Omega \mathbf{u}\cdot(-\mathbf{u}\cdot\nabla\mathbf{u}) d\mathbf{x} = 0, \tag{2.28}$$

$$\int_\Omega \mathbf{u}\cdot(-\nabla p) d\mathbf{x} = 0, \tag{2.29}$$

and

$$\int_\Omega [\mathbf{u}(\nabla\cdot\sigma) - \mathbf{H}\cdot S(\nabla\mathbf{u},\mathbf{Q})]\, d\mathbf{x} = 0. \tag{2.30}$$

Finally, we end up with

$$\frac{d\mathscr{E}}{dt} = -\int_{\Omega} \left[\eta|\nabla \mathbf{u}|^2 + M_1|\mathbf{H}|^2\right] d\mathbf{x}. \tag{2.31}$$

□

This energy dissipation property provides the foundation, as well as a guidance for us to derive semi discrete energy-stable schemes for the nematic liquid crystal model. Specifically, in the next section, we will propose a first-order and a second-order unconditional, energy-stable scheme for this model, respectively. Then, we will discuss decoupling strategies to yield two linearly, first order, decoupled energy stable schemes for the same model. The proof of stability of the schemes will be given in details in the following.

3 Semi-Discrete Numerical Schemes

To design numerical schemes and prove their energy stability, we have to assume some properties for the bulk potential function $g(\mathbf{Q})$ technically, i.e. it satisfy the following properties: (i). g has a continuous second order derivative, (ii). there exists a constant L such that

$$\max_{\mathbf{Q}\in\Lambda} |\mathcal{H}(\mathbf{Q})| \leq L, \tag{3.1}$$

where $\mathcal{H}(\mathbf{Q})$ is the Hessian matrix of $g(\mathbf{Q})$. One might immediately notice, the Landau–de Gennes bulk potential $g(\mathbf{Q})$ in (1.5) does not satisfies (3.1) as it is.

In practice, the properties can be readily met provided we modify the given function of $g(\mathbf{Q})$ far away from the origin by an essentially quadratic potential of $\mathbf{Q}$ to meet the conditions. Physically, $\mathbf{Q}$ is bounded since it is the deviatoric part of a second moment of a probability density function and the bulk potential makes sense only for $\mathbf{Q}$ being confined in its physically relevant domain. Thus, any modification of the bulk potential beyond the domain would not change the physical relevance of the model. For instance, we can propose

$$g(\mathbf{Q}) = \begin{cases} \frac{1}{2}tr(\mathbf{Q}^2) + \frac{a_2}{3}tr(\mathbf{Q}^3) + \frac{a_3}{4}(tr(\mathbf{Q}^2))^2, & tr(\mathbf{Q}^2) \leq \frac{4}{3}, \\ \frac{1}{2}tr(\mathbf{Q}^2) + \frac{a_2}{3}tr(\mathbf{Q}^3)e^{-tr(\mathbf{Q}^2)+\frac{4}{3}} + \frac{4}{9}a_3, & tr(\mathbf{Q}^2) > \frac{4}{3}. \end{cases} \tag{3.2}$$

In addition, the bulk-potential $g(\mathbf{Q})$ could be splitted into a convex part $g_c(\mathbf{Q})$, minus another convex part $g_e(\mathbf{Q})$ [29], i.e.

$$g(\mathbf{Q}) = g_c(\mathbf{Q}) - g_e(\mathbf{Q}). \tag{3.3}$$

One case is given in (2.16) and verified in Lemma 2.4. Notice to make our proof general, we don't necessarily restrict to any specific bulk potentials in the following discussion.

We next introduce the following notations:

$$\begin{aligned} \mathbf{u}^{n+\frac{1}{2}} &= \frac{1}{2}\left(\mathbf{u}^{n+1} + \mathbf{u}^n\right), \quad \mathbf{Q}^{n+\frac{1}{2}} = \frac{1}{2}\left(\mathbf{Q}^{n+1} + \mathbf{Q}^n\right), \\ \overline{\mathbf{u}}^{n+\frac{1}{2}} &= \frac{3}{2}\mathbf{u}^n - \frac{1}{2}\mathbf{u}^{n-1}, \quad \overline{\mathbf{Q}}^{n+\frac{1}{2}} = \frac{3}{2}\mathbf{Q}^n - \frac{1}{2}\mathbf{Q}^{n-1}. \end{aligned} \tag{3.4}$$

We use E^n to denote the discrete energy at time step t^n,

$$E^n = \left(\frac{K}{2}|\nabla \mathbf{Q}^n|^2 + g(\mathbf{Q}^n), 1\right), \tag{3.5}$$

and denote

$$g'(\mathbf{Q}) = \nabla_{\mathbf{Q}} g(\mathbf{Q}), \quad g''(\mathbf{Q}) = \mathcal{H}(\mathbf{Q}), \tag{3.6}$$

where $\mathcal{H}(\mathbf{Q})$ is the Hessian matrix of $g(\mathbf{Q})$.

3.1 Preliminaries

We first present some lemmas to assist readers to navigate through the details of the proof of the main theorem.

Lemma 3.1 *The following equalities hold,*

$$\begin{aligned}
2(\mathbf{Q}^{n+1} - \mathbf{Q}^n, \mathbf{Q}^{n+1}) &= \|\mathbf{Q}^{n+1}\|^2 - \|\mathbf{Q}^n\|^2 + \|\mathbf{Q}^{n+1} - \mathbf{Q}^n\|^2, \\
2(\mathbf{Q}^{n+1} - \mathbf{Q}^n, \mathbf{Q}^n) &= \|\mathbf{Q}^{n+1}\|^2 - \|\mathbf{Q}^n\|^2 - \|\mathbf{Q}^{n+1} - \mathbf{Q}^n\|^2, \\
2(\nabla\mathbf{Q}^{n+1} - \nabla\mathbf{Q}^n, \nabla\mathbf{Q}^{n+1}) &= \|\nabla\mathbf{Q}^{n+1}\|^2 - \|\nabla\mathbf{Q}^n\|^2 + \|\nabla\mathbf{Q}^{n+1} - \nabla\mathbf{Q}^n\|^2, \\
2(\nabla\mathbf{Q}^{n+1} - \nabla\mathbf{Q}^n, \nabla\mathbf{Q}^n) &= \|\nabla\mathbf{Q}^{n+1}\|^2 - \|\nabla\mathbf{Q}^n\|^2 - \|\nabla\mathbf{Q}^{n+1} - \nabla\mathbf{Q}^n\|^2.
\end{aligned} \tag{3.7}$$

Proof We can obtain the equalities by simply expanding the inner product on the right hand side and then combining the corresponding terms. □

Lemma 3.2 *Let $g \in C^2(\Lambda)$, with Λ defined by (1.1).*

(i) If

$$\max_{\mathbf{x}\in\Lambda} |\mathcal{H}(\mathbf{x})| < L, \tag{3.8}$$

where $H(\mathbf{x})$ is the Hessian matrix of $g(\mathbf{x})$, then $\forall \mathbf{x}^{n+1}, \mathbf{x}^n \in \Lambda$, the following inequality holds,

$$\left(\mathbf{x}^{n+1} - \mathbf{x}^n, \nabla_{\mathbf{x}} g(\mathbf{x}^n)\right) \geq \left(g\left(\mathbf{x}^{n+1}\right) - g\left(\mathbf{x}^n\right), 1\right) - L\|\mathbf{x}^{n+1} - \mathbf{x}^n\|^2. \tag{3.9}$$

(ii) If g is a convex function, i.e. $H(\mathbf{x})$ is positive definite $\forall \mathbf{x} \in \Lambda$, the following two inequalities hold

$$-\left(\mathbf{x}^{n+1} - \mathbf{x}^n, \nabla_{\mathbf{x}} g(\mathbf{x}^n)\right) \geq -\left(g(\mathbf{x}^{n+1}) - g(\mathbf{x}^n), 1\right) \tag{3.10}$$

$$\left(\mathbf{x}^{n+1} - \mathbf{x}^n, \nabla_{\mathbf{x}} g(\mathbf{x}^{n+1})\right) \geq \left(g(\mathbf{x}^{n+1}) - g(\mathbf{x}^n), 1\right) \tag{3.11}$$

Proof Using the Taylor expansion, $\forall \mathbf{x}^n, \mathbf{x}^{n+1} \in \Lambda$, we have

$$\begin{aligned}
g(\mathbf{x}^{n+1}) &= g(\mathbf{x}^n) + \nabla_{\mathbf{x}} g(\mathbf{x}^n)(\mathbf{x}^{n+1} - \mathbf{x}^n) \\
&\quad + (\mathbf{x}^{n+1} - \mathbf{x}^n)^T \mathcal{H}(\zeta_1)(\mathbf{x}^{n+1} - \mathbf{x}^n), \quad \zeta_1 \in \Lambda
\end{aligned} \tag{3.12}$$

$$\begin{aligned}
g(\mathbf{x}^n) &= g(\mathbf{x}^{n+1}) + \nabla_{\mathbf{x}} g(\mathbf{x}^{n+1})(\mathbf{x}^n - \mathbf{x}^{n+1}) \\
&\quad + (\mathbf{x}^n - \mathbf{x}^{n+1})^T \mathcal{H}(\zeta_2)(\mathbf{x}^n - \mathbf{x}^{n+1}), \zeta_2 \in \Lambda
\end{aligned} \tag{3.13}$$

(i) If (3.8) holds, from (3.12), we have

$$g(\mathbf{x}^{n+1}) \leq g(\mathbf{x}^n) + \nabla_{\mathbf{x}} g(\mathbf{x}^n)(\mathbf{x}^{n+1} - \mathbf{x}^n) + L|\mathbf{x}^{n+1} - \mathbf{x}^n|^2. \tag{3.14}$$

Integrating over Ω, we obtain

$$(\mathbf{x}^{n+1} - \mathbf{x}^n, \nabla_{\mathbf{x}} g(\mathbf{x}^n)) \geq (g(\mathbf{x}^{n+1}) - g(\mathbf{x}^n), 1) - L\|\mathbf{x}^{n+1} - \mathbf{x}^n\|^2. \tag{3.15}$$

(ii) If g is a convex function, from (3.12), we obtain

$$g(\mathbf{x}^{n+1}) - g(\mathbf{x}^n)) \geq (\mathbf{x}^{n+1} - \mathbf{x}^n) \cdot \nabla_{\mathbf{x}} g(\mathbf{x}^n), \tag{3.16}$$

Taking intergation over Ω, we will arrive

$$-(\mathbf{x}^{n+1}-\mathbf{x}^n, \nabla_{\mathbf{x}} g(\mathbf{x}^n)) \geq -(g(\mathbf{x}^{n+1})-g(\mathbf{x}^n), 1). \tag{3.17}$$

Analogously, from (3.13), we can derive

$$(\mathbf{x}^{n+1}-\mathbf{x}^n, \nabla_{\mathbf{x}} g(\mathbf{x}^{n+1})) \geq (g(\mathbf{x}^{n+1})-g(\mathbf{x}^n), 1). \tag{3.18}$$

□

Lemma 3.3 *Define*

$$\mathbf{H}^{n+1} = K\nabla^2\mathbf{Q}^{n+1} - g'(\mathbf{Q}^n) - C_1(\mathbf{Q}^{n+1}-\mathbf{Q}^n). \tag{3.19}$$

Then, the following inequality holds,

$$-(\mathbf{Q}^{n+1}-\mathbf{Q}^n, \mathbf{H}^{n+1}) \geq E^{n+1}-E^n, \tag{3.20}$$

provided $C_1 > L$, where E^{n+1} and E^n are the discrete free energy defined in (3.5).

Proof If $C_1 > L$, according to Lemma 3.2, we obtain

$$\begin{aligned}
-(\mathbf{Q}^{n+1}-\mathbf{Q}^n, \mathbf{H}^{n+1}) &= C_1\|\mathbf{Q}^{n+1}-\mathbf{Q}^n\|^2 + \frac{K}{2}\left(\|\nabla\mathbf{Q}^{n+1}\|^2 - \|\nabla\mathbf{Q}^n\|^2 + \|\nabla\mathbf{Q}^{n+1}-\nabla\mathbf{Q}^n\|^2\right) \\
&\quad + (\mathbf{Q}^{n+1}-\mathbf{Q}^n, g'(\mathbf{Q}^n)) \\
&\geq C_1\|\mathbf{Q}^{n+1}-\mathbf{Q}^n\|^2 + \frac{K}{2}(\|\nabla\mathbf{Q}^{n+1}\|^2 - \|\nabla\mathbf{Q}^n\|^2) \\
&\quad + (g(\mathbf{Q}^{n+1})-g(\mathbf{Q}^n), 1) - L\|\mathbf{Q}^{n+1}-\mathbf{Q}^n\|^2 \\
&\geq E^{n+1}-E^n.
\end{aligned} \tag{3.21}$$

□

Lemma 3.4 *Define*

$$\mathbf{H}^{n+\frac{1}{2}} = K\nabla^2\mathbf{Q}^{n+\frac{1}{2}} - {g_1'}^{n+\frac{1}{2}}, \tag{3.22}$$

where

$${g_1'}^{n+\frac{1}{2}} = \begin{cases} \frac{g(\mathbf{Q}^{n+1})-g(\mathbf{Q}^n)}{\mathbf{Q}^{n+1}-\mathbf{Q}^n}, & \mathbf{Q}^{n+1} \neq \mathbf{Q}^n \\ g'(\mathbf{Q}^n), & \mathbf{Q}^{n+1} = \mathbf{Q}^n. \end{cases} \tag{3.23}$$

Then,

$$-\left(\mathbf{Q}^{n+1}-\mathbf{Q}^n, \mathbf{H}^{n+\frac{1}{2}}\right) = E^{n+1}-E^n. \tag{3.24}$$

Proof We take the inner product of (3.22) with $\mathbf{Q}^{n+1}-\mathbf{Q}^n$. Then, we obtain

$$\begin{aligned}
-\left(\mathbf{Q}^{n+1}-\mathbf{Q}^n, \mathbf{H}^{n+\frac{1}{2}}\right) &= \frac{K}{2}\left(|\nabla\mathbf{Q}^{n+1}|^2 - |\nabla\mathbf{Q}^n|^2, 1\right) + \left(g\left(\mathbf{Q}^{n+1}\right) - g\left(\mathbf{Q}^n\right), 1\right) \\
&= E^{n+1}-E^n.
\end{aligned} \tag{3.25}$$

□

Lemma 3.5 *Define*

$$\mathbf{H}^{n+\frac{1}{2}} = K\nabla^2\mathbf{Q}^{n+\frac{1}{2}} - {g_2'}^{n+\frac{1}{2}}, \tag{3.26}$$

where

$$g_2'^{n+\frac{1}{2}} = g_c'\left(\mathbf{Q}^{n+1}\right) - \frac{1}{2}\left(\mathbf{Q}^{n+1} - \mathbf{Q}^n\right) g_c''\left(\mathbf{Q}^{n+1}\right) - g_e'\left(\mathbf{Q}^n\right) - \frac{1}{2}\left(\mathbf{Q}^{n+1} - \mathbf{Q}^n\right) g_e''\left(\mathbf{Q}^n\right). \tag{3.27}$$

Here we denote $g(\mathbf{Q}) = g_c(\mathbf{Q}) - g_e(\mathbf{Q})$ *with* g_c *and* g_e *are all convex functions. Then,*

$$-\left(\mathbf{Q}^{n+1} - \mathbf{Q}^n, \mathbf{H}^{n+\frac{1}{2}}\right) \geq E^{n+1} - E^n. \tag{3.28}$$

Proof Taking the inner product of (3.26) with $\mathbf{Q}^{n+1} - \mathbf{Q}^n$, we have

$$\begin{aligned}
&-\left(\mathbf{Q}^{n+1} - \mathbf{Q}^n, \mathbf{H}^{n+\frac{1}{2}}\right) \\
&= \frac{K}{2}\left(|\nabla \mathbf{Q}^{n+1}|^2 - |\nabla \mathbf{Q}^n|^2, 1\right) + \left(g_c'\left(\mathbf{Q}^{n+1}\right), \mathbf{Q}^{n+1} - \mathbf{Q}^n\right) - \left(g_e'\left(\mathbf{Q}^n\right), \mathbf{Q}^{n+1} - \mathbf{Q}^n\right) \\
&\quad + \frac{K}{2}\left(g_c''\left(\mathbf{Q}^{n+1}\right), \left(\mathbf{Q}^{n+1} - \mathbf{Q}^n\right)^2\right) + \frac{1}{2}\left(g_e''\left(\mathbf{Q}^n\right), \left(\mathbf{Q}^{n+1} - \mathbf{Q}^n\right)^2\right) \\
&\geq \frac{1}{2}\left(|\nabla \mathbf{Q}^{n+1}|^2 - |\nabla \mathbf{Q}^n|^2, 1\right) + \left(g_c'\left(\mathbf{Q}^{n+1}\right), \mathbf{Q}^{n+1} - \mathbf{Q}^n\right) - \left(g_e'\left(\mathbf{Q}^n\right), \mathbf{Q}^{n+1} - \mathbf{Q}^n\right),
\end{aligned} \tag{3.29}$$

since g_c and g_e are convex functions. Using Lemma 3.2, we arrive at

$$\begin{aligned}
&-\left(\mathbf{Q}^{n+1} - \mathbf{Q}^n, \mathbf{H}^{n+\frac{1}{2}}\right) \\
&\geq \frac{K}{2}\left(|\nabla \mathbf{Q}^{n+1}|^2 - |\nabla \mathbf{Q}^n|^2, 1\right) + \left(g_c\left(\mathbf{Q}^{n+1}\right) - g_c\left(\mathbf{Q}^n\right), 1\right) - \left(g_e\left(\mathbf{Q}^{n+1}\right) - g_e\left(\mathbf{Q}^n\right), 1\right) \\
&= E^{n+1} - E^n.
\end{aligned} \tag{3.30}$$

□

3.2 First-Order, Coupled Unconditionally Energy Stable Schemes

Here, we present a first-order, coupled, linear, unconditionally energy stable scheme.

Given the initial condition $\mathbf{Q}^0, \mathbf{u}^0$ *and* $p^0 = 0$ *and having computed* $(\mathbf{Q}^n, \mathbf{u}^n, p^n)$, *we calculate* $(\mathbf{Q}^{n+1}, \mathbf{u}^{n+1}, p^{n+1})$ *in the following two steps,*

(1) Step 1: update $(\mathbf{Q}^{n+1}, \mathbf{u}_\star^{n+1})$:

$$\begin{cases}
\frac{\mathbf{Q}^{n+1} - \mathbf{Q}^n}{\delta t} + \mathbf{u}_\star^{n+1} \cdot \nabla \mathbf{Q}^n - S\left(\nabla \mathbf{u}_\star^{n+1}, \mathbf{Q}^n\right) = M_1 \mathbf{H}^{n+1}, \\
\mathbf{H}^{n+1} = -C_1\left(\mathbf{Q}^{n+1} - \mathbf{Q}^n\right) + K\nabla^2 \mathbf{Q}^{n+1} - g'\left(\mathbf{Q}^n\right), \\
\frac{\mathbf{u}_\star^{n+1} - \mathbf{u}^n}{\delta t} + \left(\mathbf{u}^n \cdot \nabla\right)\mathbf{u}_\star^{n+1} = \eta \Delta \mathbf{u}_\star^{n+1} - \nabla p^n + \nabla \cdot \sigma\left(\mathbf{Q}^n, \mathbf{H}^{n+1}\right) - \mathbf{H}^{n+1}\nabla \mathbf{Q}^n \\
\mathbf{u}_\star^{n+1}|_{\partial\Omega} = 0, \quad \frac{\partial \mathbf{Q}^{n+1}}{\partial \mathbf{n}}|_{\partial\Omega} = 0,
\end{cases} \tag{3.31}$$

(2) Step 2: update $\mathbf{u}^{n+1}$:

$$\begin{cases}
\frac{\mathbf{u}^{n+1} - \mathbf{u}_\star^{n+1}}{\delta t} = -\nabla\left(p^{n+1} - p^n\right), \\
\nabla \cdot \mathbf{u}^{n+1} = 0, \quad \mathbf{u}^{n+1} \cdot \mathbf{n}|_{\partial\Omega} = 0.
\end{cases} \tag{3.32}$$

Theorem 3.1 *Given $C_1 \geq L$, the scheme (3.31)–(3.32) obeys the discrete energy law*

$$\frac{1}{2}\|\mathbf{u}^{n+1}\|^2 + E^{n+1} + \frac{\delta t^2}{2}\|\nabla p^{n+1}\|^2 + \delta t\left(\eta\|\nabla \mathbf{u}_\star^{n+1}\|^2 + M_1\|\mathbf{H}^{n+1}\|^2\right) \leq \frac{1}{2}\|\mathbf{u}^n\|^2 + E^n + \frac{\delta t^2}{2}\|\nabla p^n\|^2, \tag{3.33}$$

where E^n and E^{n+1} are defined in (3.5).

Proof Taking the inner-product of (3.31) with $2\delta t\mathbf{u}_\star^{n+1}$, we obtain,

$$\|\mathbf{u}_\star^{n+1}\|^2 - \|\mathbf{u}^n\|^2 + \|\mathbf{u}_\star^{n+1} - \mathbf{u}^n\|^2 + 2\eta\delta t\|\nabla \mathbf{u}_\star^{n+1}\|^2 + 2\delta t\left(\nabla p^n, \mathbf{u}_\star^{n+1}\right) + 2\delta t\left(\mathbf{H}^{n+1}\nabla \mathbf{Q}^n, \mathbf{u}_\star^n\right)\big) - 2\delta t\left(\nabla\cdot\sigma(\mathbf{Q}^n, \mathbf{H}^{n+1}), \mathbf{u}_\star^n\right) = 0. \tag{3.34}$$

To deal with the pressure term, we take the inner product of (3.32) with $2\delta t^2\nabla p^n$ to arrive at

$$\delta t^2(\|\nabla p^{n+1}\|^2 - \|\nabla p^n\|^2 - \|\nabla p^{n+1} - \nabla p^n\|^2) = 2\delta t(\mathbf{u}_\star^{n+1}, \nabla p^n). \tag{3.35}$$

Taking the inner product of (3.32) with $2\delta t\mathbf{u}^{n+1}$, we obtain

$$\|\mathbf{u}^{n+1}\|^2 + \|\mathbf{u}^{n+1} - \mathbf{u}_\star^{n+1}\|^2 = \|\mathbf{u}_\star^{n+1}\|^2. \tag{3.36}$$

It follows from (3.32) directly that

$$\delta t^2\|\nabla p^{n+1} - \nabla p^n\|^2 = \|\mathbf{u}_\star^{n+1} - \mathbf{u}^{n+1}\|^2. \tag{3.37}$$

Combining (3.34)–(3.37), we obtain

$$\|\mathbf{u}^{n+1}\|^2 - \|\mathbf{u}^{n+1}\|^2 + \|\mathbf{u}_\star^{n+1} - \mathbf{u}^n\|^2 + \delta t^2\left(\|\nabla p^{n+1}\|^2 - \|\nabla p^n\|^2\right) + 2\eta\delta t\|\nabla \mathbf{u}_\star^{n+1}\|^2 + 2\delta t\left(\mathbf{H}^{n+1}\nabla \mathbf{Q}^n, \mathbf{u}_\star^n\right) - 2\delta t\left(\nabla\cdot\sigma(\mathbf{Q}^n, \mathbf{H}^{n+1}), \mathbf{u}_\star^{n+1}\right) = 0. \tag{3.38}$$

If we take the inner product of (3.31) with $2\delta t\mathbf{H}^{n+1}$, we get

$$2\delta t M_1\|\mathbf{H}^{n+1}\|^2 - 2\delta t(\mathbf{H}^{n+1}, (\mathbf{u}_\star^{n+1}\cdot\nabla)\mathbf{Q}^n) - 2(\mathbf{Q}^{n+1} - \mathbf{Q}^n, \mathbf{H}^{n+1}) + 2\delta t\left(\mathbf{H}^{n+1}, S(\nabla \mathbf{u}_\star^{n+1}, \mathbf{Q}^n)\right) = 0. \tag{3.39}$$

Applying Lemma 2.3, we have

$$\left(\nabla\cdot\sigma(\mathbf{Q}^n, \mathbf{H}^{n+1}), \mathbf{u}_\star^{n+1}\right) = \left(\mathbf{H}^{n+1}, S(\nabla \mathbf{u}_\star^{n+1}, \mathbf{Q}^n)\right), \tag{3.40}$$

Then adding (3.38) and (3.39) and using the equality (3.40), we obtain

$$\|\mathbf{u}^{n+1}\|^2 - \|\mathbf{u}^{n+1}\|^2 + \|\mathbf{u}_\star^{n+1} - \mathbf{u}^n\|^2 + \delta t^2\left(\|\nabla p^{n+1}\|^2 - \|\nabla p^n\|^2\right) + 2\eta\delta t\|\nabla \mathbf{u}_\star^{n+1}\|^2 + 2\delta t M_1\|\mathbf{H}^{n+1}\|^2 - 2\left(\mathbf{Q}^{n+1} - \mathbf{Q}^n, \mathbf{H}^{n+1}\right) = 0. \tag{3.41}$$

Applying Lemma 3.3, we finally arrive at

$$\frac{1}{2}\|\mathbf{u}^{n+1}\|^2 + E^{n+1} + \frac{\delta t^2}{2}\|\nabla p^{n+1}\|^2 + \delta t\left(\eta\|\nabla \mathbf{u}_\star^{n+1}\|^2 + M_1\|\mathbf{H}^{n+1}\|^2\right) \leq \frac{1}{2}\|\mathbf{u}^n\|^2 + E^n + \frac{\delta t^2}{2}\|\nabla p^n\|^2. \tag{3.42}$$

□

Remark 3.1 In scheme (3.31)–(3.32), we use the first-order pressure correction scheme to handle the momentum transport equation together with the incompressibility condition. This scheme is thus first-order and energy stable. We notice that there exists a coupling between $\mathbf{Q}^{n+1}$ and $\mathbf{u}_\star^{n+1}$, which means that we have to solve these two equations simultaneously. We will design schemes to decouple them in the following.

Remark 3.2 C_1 term is the added first-order stabilizer to balance the explicit treatment for $g(\mathbf{Q})$ [21,31]. One can also use the convex splitting strategy to deal with such a nonlinear term [19] without introducing the order one term.

3.3 Second-Order, Coupled Unconditionally Energy Stable Schemes

In a similar way, we now design a second-order, coupled, unconditionally energy stable scheme.

Given the initial condition $\mathbf{Q}^0, \mathbf{u}^0$ *and* $p^0 = 0$, *we first compute* $\mathbf{Q}^1, \mathbf{u}^1$ *and* p^1 *by the first-order scheme* (3.31)–(3.32). *Having computed* $(\mathbf{Q}^{n-1}, \mathbf{u}^{n-1}, p^{n-1})$ *and* $(\mathbf{Q}^n, \mathbf{u}^n, p^n)$, *where* $n \geq 2$, *we calculate* $(\mathbf{Q}^{n+1}, \mathbf{u}^{n+1}, p^{n+1})$ *in the following two steps*:

(1) Step 1: update $(\mathbf{Q}^{n+1}, \mathbf{u}_\star^{n+1})$:

$$\begin{cases} \frac{\mathbf{Q}^{n+1}-\mathbf{Q}^n}{\delta t} + \mathbf{u}_\star^{n+\frac{1}{2}} \cdot \nabla \overline{\mathbf{Q}}^{n+\frac{1}{2}} - S\left(\nabla \mathbf{u}_\star^{n+\frac{1}{2}}, \overline{\mathbf{Q}}^{n+\frac{1}{2}}\right) = M_1 \mathbf{H}^{n+\frac{1}{2}}, \\ \mathbf{H}^{n+\frac{1}{2}} = K\nabla^2 \mathbf{Q}^{n+\frac{1}{2}} - g'^{n+\frac{1}{2}}, \\ \frac{\mathbf{u}_\star^{n+1}-\mathbf{u}^n}{\delta t} + \left(\overline{\mathbf{u}}^{n+\frac{1}{2}} \cdot \nabla\right) \mathbf{u}_\star^{n+\frac{1}{2}} = \eta \Delta \mathbf{u}_\star^{n+\frac{1}{2}} - \nabla p^n + \nabla \cdot \sigma\left(\overline{\mathbf{Q}}^{n+\frac{1}{2}}, \mathbf{H}^{n+\frac{1}{2}}\right) \\ \qquad\qquad - \mathbf{H}^{n+\frac{1}{2}} \nabla \overline{\mathbf{Q}}^{n+\frac{1}{2}}, \\ \mathbf{u}_\star^{n+1}|_{\partial\Omega} = 0, \quad \frac{\partial \mathbf{Q}^{n+1}}{\partial \mathbf{n}}|_{\partial\Omega} = 0, \mathbf{u}_\star^{n+\frac{1}{2}} = \frac{1}{2}\left(\mathbf{u}_\star^{n+1} + \mathbf{u}^n\right), \end{cases} \tag{3.43}$$

where $\tilde{g}^{n+\frac{1}{2}}$ *is a second-order approximation for* $g(\mathbf{Q}^{n+\frac{1}{2}})$. *We will give a detailed discussion on choices of* $\tilde{g}$.

(2) Step 2: update $\mathbf{u}^{n+1}$:

$$\begin{cases} \frac{\mathbf{u}^{n+1}-\mathbf{u}_\star^{n+1}}{\delta t} = -\frac{1}{2}\nabla\left(p^{n+1} - p^n\right), \\ \nabla \cdot \mathbf{u}^{n+1} = 0, \quad \mathbf{u}^{n+1} \cdot \mathbf{n}|_{\partial\Omega} = 0. \end{cases} \tag{3.44}$$

Theorem 3.2 *Given*

$$g'^{n+\frac{1}{2}} = \begin{cases} \frac{g(\mathbf{Q}^{n+1})-g(\mathbf{Q}^n)}{\mathbf{Q}^{n+1}-\mathbf{Q}^n}, & \mathbf{Q}^{n+1} \neq \mathbf{Q}^n \\ g'(\mathbf{Q}^n), & \mathbf{Q}^{n+1} = \mathbf{Q}^n, \end{cases} \tag{3.45}$$

the scheme (3.43)–(3.44) *obeys the discrete energy law*

$$\begin{aligned} &\frac{1}{2}\|\mathbf{u}^{n+1}\|^2 + E^{n+1} + \frac{\delta t^2}{8}\|\nabla p^{n+1}\|^2 + \delta t\left(\eta\|\nabla \mathbf{u}_\star^{n+\frac{1}{2}}\|^2 + M_1\|\mathbf{H}^{n+\frac{1}{2}}\|^2\right) \\ &= \frac{1}{2}\|\mathbf{u}^n\|^2 + E^n + \frac{\delta t^2}{8}\|\nabla p^n\|^2, \end{aligned} \tag{3.46}$$

where E^n *and* E^{n+1} *are defined in* (3.5).

Proof The proof is similar to the one in the previous theorem. Nevertheless, we provide some details below. Taking the inner-product of (3.43) with $2\delta t\mathbf{u}_\star^{n+\frac{1}{2}}$, we obtain,

$$\|\mathbf{u}_\star^{n+1}\|^2 - \|\mathbf{u}^n\|^2 + 2\eta\delta t\|\nabla\mathbf{u}_\star^{n+\frac{1}{2}}\|^2 + 2\delta t\left(\nabla p^n, \mathbf{u}_\star^{n+\frac{1}{2}}\right) + 2\delta t\left(\mathbf{H}^{n+\frac{1}{2}}\nabla\overline{\mathbf{Q}}^{n+\frac{1}{2}}, \mathbf{u}_\star^{n+\frac{1}{2}}\right) - 2\delta t\left(\nabla\cdot\sigma(\overline{\mathbf{Q}}^{n+\frac{1}{2}}, \mathbf{H}^{n+\frac{1}{2}}), \mathbf{u}_\star^{n+\frac{1}{2}}\right) = 0. \quad (3.47)$$

To deal with the pressure term, we take the inner product of (3.44) with $2\delta t^2\nabla p^n$ to arrive at

$$\frac{\delta t^2}{4}\left(\|\nabla p^{n+1}\|^2 - \|\nabla p^n\|^2 - \|\nabla p^{n+1} - \nabla p^n\|^2\right) = \delta t\left(\mathbf{u}_\star^{n+1}, \nabla p^n\right). \quad (3.48)$$

Taking the inner product of (3.44) with $2\delta t\mathbf{u}^{n+1}$, we obtain

$$\|\mathbf{u}^{n+1}\|^2 + \|\mathbf{u}^{n+1} - \mathbf{u}_\star^{n+1}\|^2 = \|\mathbf{u}_\star^{n+1}\|^2. \quad (3.49)$$

It follows from (3.44) directly that

$$\frac{\delta t^2}{4}\|\nabla p^{n+1} - \nabla p^n\|^2 = \|\mathbf{u}_\star^{n+1} - \mathbf{u}^{n+1}\|^2. \quad (3.50)$$

Noticing the fact

$$2\delta t\left(\nabla p^n, \mathbf{u}_\star^{n+\frac{1}{2}}\right) = \delta t\left(\nabla p^n, \mathbf{u}_\star^{n+1}\right), \quad (3.51)$$

(due to $(\nabla p, \mathbf{u}^n) = 0$), and combining (3.47)–(3.50), we obtain

$$\|\mathbf{u}^{n+1}\|^2 - \|\mathbf{u}^n\|^2 + \frac{\delta t^2}{4}\left(\|\nabla p^{n+1}\|^2 - \|\nabla p^n\|^2\right) + 2\eta\delta t\|\nabla\mathbf{u}_\star^{n+1}\|^2 + 2\delta t\left(\mathbf{H}^{n+\frac{1}{2}}\nabla\overline{\mathbf{Q}}^{n+\frac{1}{2}}, \mathbf{u}_\star^{n+\frac{1}{2}}\right) - 2\delta t\left(\nabla\cdot\sigma(\overline{\mathbf{Q}}^{n+\frac{1}{2}}, \mathbf{H}^{n+\frac{1}{2}}), \mathbf{u}_\star^{n+\frac{1}{2}}\right) = 0. \quad (3.52)$$

If we take the inner product of (3.43) with $2\delta t\mathbf{H}^{n+\frac{1}{2}}$, we get

$$2\delta t M_1\|\mathbf{H}^{n+\frac{1}{2}}\|^2 - 2\delta t\left(\mathbf{H}^{n+\frac{1}{2}}, \left(\mathbf{u}_\star^{n+\frac{1}{2}}\cdot\nabla\right)\mathbf{Q}^{n+\frac{1}{2}}\right) - 2\left(\mathbf{Q}^{n+1} - \mathbf{Q}^n, \mathbf{H}^{n+\frac{1}{2}}\right) + 2\delta t\left(\mathbf{H}^{n+\frac{1}{2}}, S(\nabla\mathbf{u}_\star^{n+\frac{1}{2}}, \overline{\mathbf{Q}}^{n+\frac{1}{2}})\right) = 0. \quad (3.53)$$

Applying Lemma 3.3, i.e.

$$\left(\nabla\cdot\sigma(\overline{\mathbf{Q}}^{n+\frac{1}{2}}, \mathbf{H}^{n+\frac{1}{2}}), \mathbf{u}_\star^{n+\frac{1}{2}}\right) = \left(\mathbf{H}^{n+\frac{1}{2}}, S(\nabla\mathbf{u}_\star^{n+\frac{1}{2}}, \overline{\mathbf{Q}}^{n+\frac{1}{2}})\right), \quad (3.54)$$

and adding (3.52) and (3.53), we obtain

$$\|\mathbf{u}^{n+1}\|^2 - \|\mathbf{u}^n\|^2 + \frac{\delta t^2}{4}\left(\|\nabla p^{n+1}\|^2 - \|\nabla p^n\|^2\right) + 2\eta\delta t\|\nabla\mathbf{u}_\star^{n+1}\|^2 + 2\delta t M_1\|\mathbf{H}^{n+\frac{1}{2}}\|^2 - 2\left(\mathbf{Q}^{n+1} - \mathbf{Q}^n, \mathbf{H}^{n+\frac{1}{2}}\right) = 0. \quad (3.55)$$

From Lemma 3.4, we have

$$-\left(\mathbf{Q}^{n+1} - \mathbf{Q}^n, \mathbf{H}^{n+\frac{1}{2}}\right) = E^{n+1} - E^n. \quad (3.56)$$

Finally, we arrive at

$$\frac{1}{2}\|\mathbf{u}^{n+1}\|^2 + E^{n+1} + \frac{\delta t^2}{8}\|\nabla p^{n+1}\|^2 + \delta t\left(\eta\|\nabla \mathbf{u}_\star^{n+\frac{1}{2}}\|^2 + M_1\|\mathbf{H}^{n+\frac{1}{2}}\|^2\right)$$
$$= \frac{1}{2}\|\mathbf{u}^{n}\|^2 + E^{n} + \frac{\delta t^2}{8}\|\nabla p^{n}\|^2. \tag{3.57}$$

□

We can take advantage of the convex splitting strategy [12] to reduce the non-linear terms. Furthermore, we can also truncate the bulk potential and rewrite $g(\mathbf{Q})$ as a convex function minus another convex function. This leads to the following theorem.

Theorem 3.3 *If we define*

$$g'^{n+\frac{1}{2}} = g_c'\left(\mathbf{Q}^{n+1}\right) - \frac{1}{2}\left(\mathbf{Q}^{n+1} - \mathbf{Q}^n\right) g_c''\left(\mathbf{Q}^{n+1}\right) - g_e'\left(\mathbf{Q}^n\right) - \frac{1}{2}\left(\mathbf{Q}^{n+1} - \mathbf{Q}^n\right) g_e''\left(\mathbf{Q}^n\right), \tag{3.58}$$

the scheme (3.43)–(3.44) *obeys the discrete energy law*

$$\frac{1}{2}\|\mathbf{u}^{n+1}\|^2 + E^{n+1} + \frac{\delta t^2}{8}\|\nabla p^{n+1}\|^2 + \delta t\left(\eta\|\nabla \mathbf{u}_\star^{n+\frac{1}{2}}\|^2 + M_1\|\mathbf{H}^{n+\frac{1}{2}}\|^2\right)$$
$$\leq \frac{1}{2}\|\mathbf{u}^{n}\|^2 + E^{n} + \frac{\delta t^2}{8}\|\nabla p^{n}\|^2. \tag{3.59}$$

with E^n *and* E^{n+1} *given in* (3.5).

Proof This proof is similar to the one in Theorem 3.2 except that we need to use Lemma 3.5 instead of Lemma 3.4. We thus omit the details. □

3.4 Linearly, First-Order Decoupled Energy Stable Schemes

Next, we discuss two ways to design decoupled energy stable schemes and remark on the difficulties to arrive at sharp results.

Given the initial condition $\mathbf{Q}^0, \mathbf{u}^0$ *and* $p^0 = 0$ *and having computed* $(\mathbf{Q}^n, \mathbf{u}^n, p^n)$, *where* $n \geq 1$, *we calculate* $(\mathbf{Q}^{n+1}, \mathbf{u}^{n+1}, p^{n+1})$ *in the following three steps,*

(1) Step 1: update $\mathbf{Q}^{n+1}$:

$$\begin{cases} \frac{\mathbf{Q}^{n+1}-\mathbf{Q}^n}{\delta t} + \mathbf{u}^n \cdot \nabla \mathbf{Q}^n - S\left(\nabla \mathbf{u}^n, \mathbf{Q}^n\right) = M_1 \mathbf{H}^{n+1} \\ \mathbf{H}^{n+1} = -C_1\left(\mathbf{Q}^{n+1} - \mathbf{Q}^n\right) + K\nabla^2 \mathbf{Q}^{n+1} - g'\left(\mathbf{Q}^n\right), \\ \frac{\partial \mathbf{Q}^{n+1}}{\partial \mathbf{n}}|_{\partial\Omega} = 0, \end{cases} \tag{3.60}$$

(2) Step 2: update intermediate variable $\mathbf{u}_\star^n$ *and* Γ^n:

$$\begin{aligned} \beta^n &= \| - \mathbf{H}^{n+1}\nabla \mathbf{Q}^n + \nabla \cdot \sigma\left(\mathbf{Q}^n, \mathbf{H}^{n+1}\right)\|, \\ \mathbf{u}_\star^n &= \mathbf{u}^n - \delta t \mathbf{H}^{n+1}\nabla \mathbf{Q}^n + \delta t \nabla \cdot \sigma\left(\mathbf{Q}^n, \mathbf{H}^{n+1}\right), \\ \Gamma^n &= -\frac{\delta t (\beta^n)^2}{\|\mathbf{u}_\star^n\|^2}\mathbf{u}_\star^n. \end{aligned} \tag{3.61}$$

(3) Step 3: update $\mathbf{u}^{n+1}$:

$$\begin{cases} \frac{\tilde{\mathbf{u}}^{n+1}-\mathbf{u}^n}{\delta t}+(\mathbf{u}^n\cdot\nabla)\tilde{\mathbf{u}}^{n+1}=\eta\Delta\tilde{\mathbf{u}}^{n+1}-\nabla p^n+\nabla\cdot\sigma\left(\mathbf{Q}^n,\mathbf{H}^{n+1}\right)-\mathbf{H}^{n+1}\nabla\mathbf{Q}^n+\Gamma^n \\ \tilde{\mathbf{u}}^{n+1}|_{\partial\Omega}=0. \end{cases} \tag{3.62}$$

$$\begin{cases} \frac{\mathbf{u}^{n+1}-\tilde{\mathbf{u}}^{n+1}}{\delta t}=-\nabla\left(p^{n+1}-p^n\right), \\ \nabla\cdot\mathbf{u}^{n+1}=0,\quad \mathbf{u}^{n+1}\cdot\mathbf{n}|_{\partial\Omega}=0. \end{cases} \tag{3.63}$$

Theorem 3.4 *Given* $C_1 > L$, *the scheme given by* (3.60)–(3.63) *satisfies the following semi-discrete energy dissipation law:*

$$\begin{aligned} &\frac{1}{2}\|\mathbf{u}^{n+1}\|^2+E^{n+1}+\frac{\delta t^2}{2}\|\nabla p^{n+1}\|^2+\delta t\left(\eta\|\nabla\tilde{\mathbf{u}}^{n+1}\|^2+M_1\|\mathbf{H}^{n+1}\|^2\right) \\ &\quad\le\frac{1}{2}\|\mathbf{u}^n\|^2+E^n+\frac{\delta t^2}{2}\|\nabla p^n\|^2+\delta t^4C^{n+1}, \end{aligned} \tag{3.64}$$

where the semi-discrete energy E^n *is defined in* (3.5) *and*

$$C^{n+1}=\frac{\|-\mathbf{H}^{n+1}\nabla\mathbf{Q}^n+\nabla\cdot\sigma\left(\mathbf{Q}^n,\mathbf{H}^{n+1}\right)\|^4}{\|\mathbf{u}^n-\delta t\mathbf{H}^{n+1}\nabla\mathbf{Q}^n+\delta t\nabla\cdot\sigma\left(\mathbf{Q}^n,\mathbf{H}^{n+1}\right)\|^2}. \tag{3.65}$$

Proof From the definition of $\mathbf{u}_\star^n$ in equation (3.61), we rewrite the momentum equation as follows

$$\mathbf{u}_\star^n=\mathbf{u}^n-\delta t\mathbf{H}^{n+1}\nabla\mathbf{Q}^n+\delta t\nabla\cdot\sigma\left(\mathbf{Q}^n,\mathbf{H}^{n+1}\right), \tag{3.66}$$

$$\mathbf{u}_{\star\star}^n=\mathbf{u}_\star^n-\delta t\Gamma^n, \tag{3.67}$$

$$\frac{\tilde{\mathbf{u}}^{n+1}-\mathbf{u}_{\star\star}^n}{\delta t}+(\mathbf{u}^n\cdot\nabla)\tilde{\mathbf{u}}^{n+1}-\eta\nabla\tilde{\mathbf{u}}^{n+1}+\nabla p^n=0. \tag{3.68}$$

If we take the inner product of (3.60) with $2\delta t\mathbf{H}^{n+1}$, we get

$$\begin{aligned} &2\delta tM_1\|\mathbf{H}^{n+1}\|^2-2\delta t(\mathbf{H}^{n+1},(\mathbf{u}^n\cdot\nabla)\mathbf{Q}^n)-2(\mathbf{Q}^{n+1}-\mathbf{Q}^n,\mathbf{H}^{n+1}) \\ &+2\delta t\left(\mathbf{H}^{n+1},(\mathbf{W}^n+a\mathbf{D}^n)\cdot\mathbf{Q}^n\right)=0. \end{aligned} \tag{3.69}$$

Taking the inner product of (3.61) with $2\mathbf{u}^n$, we obtain

$$\|\mathbf{u}_\star^n\|^2-\|\mathbf{u}^n\|^2-\|\mathbf{u}_\star^n-\mathbf{u}^n\|^2-2\delta t(\mathbf{H}^{n+1}\nabla\mathbf{Q}^n,\mathbf{u}^n))-\delta t\left(\nabla\cdot\sigma(\mathbf{Q}^n,\mathbf{H}^{n+1}),\mathbf{u}^n\right)=0. \tag{3.70}$$

From,

$$\mathbf{u}_{\star\star}^n=\mathbf{u}_\star^n+\delta t\Gamma^n, \tag{3.71}$$

we arrive at

$$\|\mathbf{u}_{\star\star}^n\|^2=\left(1-\frac{\delta t^2(\beta^n)^2}{\|\mathbf{u}_\star^n\|^2}\right)^2\|\mathbf{u}_\star^n\|^2, \tag{3.72}$$

i.e.

$$\|\mathbf{u}_{\star\star}^n\|^2-\|\mathbf{u}_\star\|^2+\delta t^2(\beta^n)^2+\delta t^2(\beta^n)^2\left(1-\tfrac{\delta t^2(\beta^n)^2}{\|\mathbf{u}_\star^n\|^2}\right)=0. \tag{3.73}$$

Notice the fact $\delta t^2(\beta^n)^2=\|\mathbf{u}_\star^n-\mathbf{u}^n\|^2$ and if we denote

$$C^{n+1}=\frac{\|-\mathbf{H}^{n+1}\nabla\mathbf{Q}^n+\nabla\cdot\sigma(\mathbf{Q}^n,\mathbf{H}^{n+1})\|^4}{\|\mathbf{u}^n-\delta t\mathbf{H}^{n+1}\nabla\mathbf{Q}^n+\delta t\nabla\cdot\sigma(\mathbf{Q}^n,\mathbf{H}^{n+1})\|^2}, \tag{3.74}$$

we obtain

$$\|\mathbf{u}_{\star\star}^n\|^2 - \|\mathbf{u}_{\star}^n\|^2 + 2\|\mathbf{u}_{\star}^n - \mathbf{u}^n\|^2 - C^{n+1}\delta t^4 = 0. \tag{3.75}$$

Taking the inner-product of (3.68) with $2\delta t\tilde{\mathbf{u}}^{n+1}$, we obtain,

$$\|\tilde{\mathbf{u}}^{n+1}\|^2 - \|\mathbf{u}_{\star\star}^n\|^2 + \|\tilde{\mathbf{u}}^{n+1} - \mathbf{u}_{\star\star}^n\|^2 + 2\eta\delta\|\nabla\tilde{\mathbf{u}}^{n+1}\|^2 + 2\delta t(\nabla p^n, \tilde{\mathbf{u}}^{n+1}) = 0. \tag{3.76}$$

To deal with the pressure term, we take the inner product of (3.63) with $2\delta t^2\nabla p^n$ to arrive at

$$\delta t^2(\|\nabla p^{n+1}\|^2 - \|\nabla p^n\|^2 - \|\nabla p^{n+1} - \nabla p^n\|^2) = 2\delta t(\tilde{\mathbf{u}}^{n+1}, \nabla p^n). \tag{3.77}$$

Taking the inner product of (3.63) with $\mathbf{u}^{n+1}$, we obtain

$$\|\mathbf{u}^{n+1}\|^2 + \|\mathbf{u}^{n+1} - \tilde{\mathbf{u}}^{n+1}\|^2 = \|\tilde{\mathbf{u}}^{n+1}\|^2. \tag{3.78}$$

It follows from (3.63) directly that

$$\delta t^2\|\nabla p^{n+1} - \nabla p^n\|^2 = \|\tilde{\mathbf{u}}^{n+1} - \mathbf{u}^{n+1}\|^2. \tag{3.79}$$

Combining (3.75) and (3.76)–(3.79), we obtain

$$\begin{aligned}&\|\mathbf{u}^{n+1}\|^2 - \|\mathbf{u}_{\star}^{n+1}\|^2 + \|\mathbf{u}_{\star}^{n+1} - \mathbf{u}^n\|^2 + \|\tilde{\mathbf{u}}^{n+1} - \mathbf{u}_{\star\star}^n\| + \delta t^2(\|\nabla p^{n+1}\|^2 - \|\nabla p^n\|^2)\\ &+ 2\eta\delta t\|\nabla\mathbf{u}_{\star}^{n+1}\|^2 - 2\delta t\left(\nabla\cdot\sigma(\mathbf{Q}^n, \mathbf{H}^{n+1}), \mathbf{u}_{\star}^n\right) - C^{n+1}\delta t^4 = 0.\end{aligned} \tag{3.80}$$

Adding (3.69) with (3.70) and noticing the fact that

$$\left(\nabla\cdot\sigma(\mathbf{Q}^n, \mathbf{H}^{n+1}), \mathbf{u}^n\right) = \left(\mathbf{H}^{n+1}, S(\nabla\mathbf{u}^n, \mathbf{Q}^n)\right), \tag{3.81}$$

we arrive at

$$\|\mathbf{u}_{\star}^n\|^2 - \|\mathbf{u}^n\|^2 + \|\mathbf{u}_{\star}^n - \mathbf{u}^n\|^2 + 2\delta t M_1\|\mathbf{H}^{n+1}\|^2 - 2(\mathbf{Q}^{n+1} - \mathbf{Q}^n, \mathbf{H}^{n+1}) = 0. \tag{3.82}$$

Finally, adding up the Eqs. (3.80), (3.82) and dividing both side by 2, we have

$$\begin{aligned}&\frac{1}{2}\left(\|\mathbf{u}^{n+1}\|^2 - \|\mathbf{u}^n\|^2 + \|\tilde{\mathbf{u}}^{n+1} - \mathbf{u}_{\star\star}^n\|^2 + \|\mathbf{u}_{\star}^{n+1} - \mathbf{u}^n\|^2\right) + \frac{1}{2}\delta t^2(\|\nabla p^{n+1}\| - \|\nabla p^n\|^2)\\ &+ \eta\delta t\|\nabla\tilde{\mathbf{u}}^{n+1}\|^2 + \delta t M_1\|\mathbf{H}^{n+1}\|^2 - (\mathbf{Q}^{n+1} - \mathbf{Q}^n, \mathbf{H}^{n+1}) - C^{n+1}\delta t^4 = 0.\end{aligned} \tag{3.83}$$

According to Lemma 3.3,

$$(\mathbf{Q}^{n+1} - \mathbf{Q}^n, \mathbf{H}^{n+1}) \geq E^{n+1} - E^n, \tag{3.84}$$

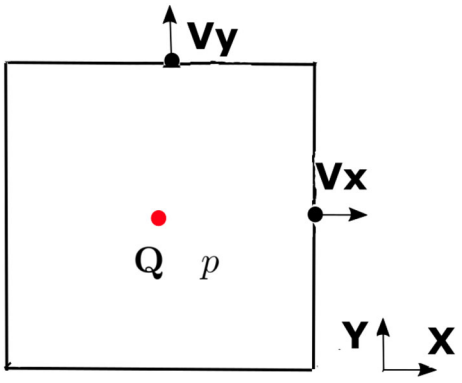

Fig. 1 A schematic of a 2D stagged grid

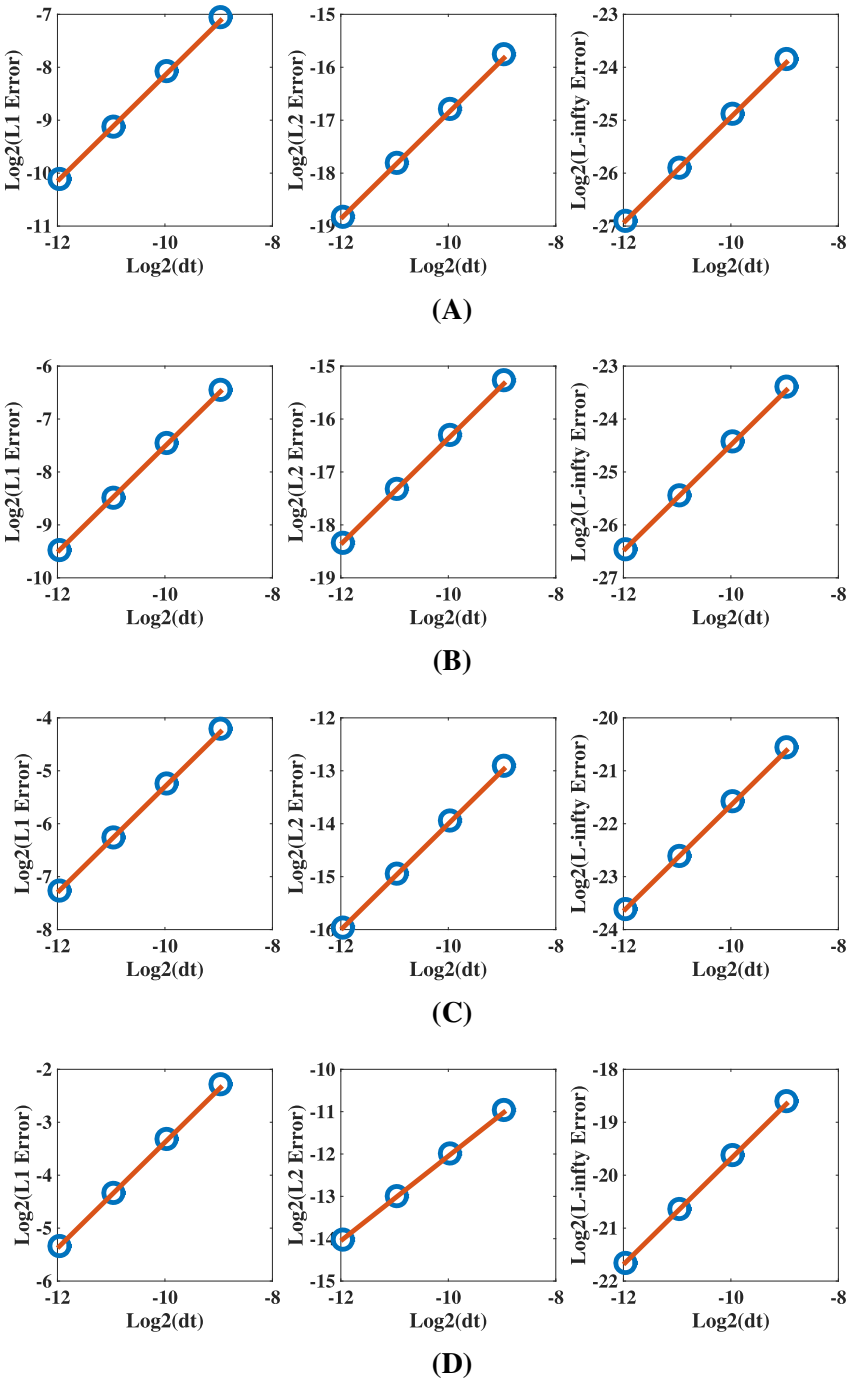

Fig. 2 Time step mesh refinement test for the 1st order scheme. Here, we use spatial mesh size 512×512 and choose time step $\delta t = 2\times10^{-3}, 10^{-3}, 5\times10^{-4}, 2.5\times10^{-4}, 1.25\times10^{-4}$, respectively. The $\log_2(L_1,\ L_2,\ L_\infty$ norm of the error) for $\mathbf{v}$ and $\mathbf{Q}_{xx}$, $\mathbf{Q}_{xy}$ versus $\log_2(\delta t)$ are plotted. The slopes of the lines are all equal to 1. **a** Error of $\mathbf{v}_x$. **b** Error of $\mathbf{v}_y$. **c** Error of $\mathbf{Q}_{xx}$. **d** Error of $\mathbf{Q}_{xy}$

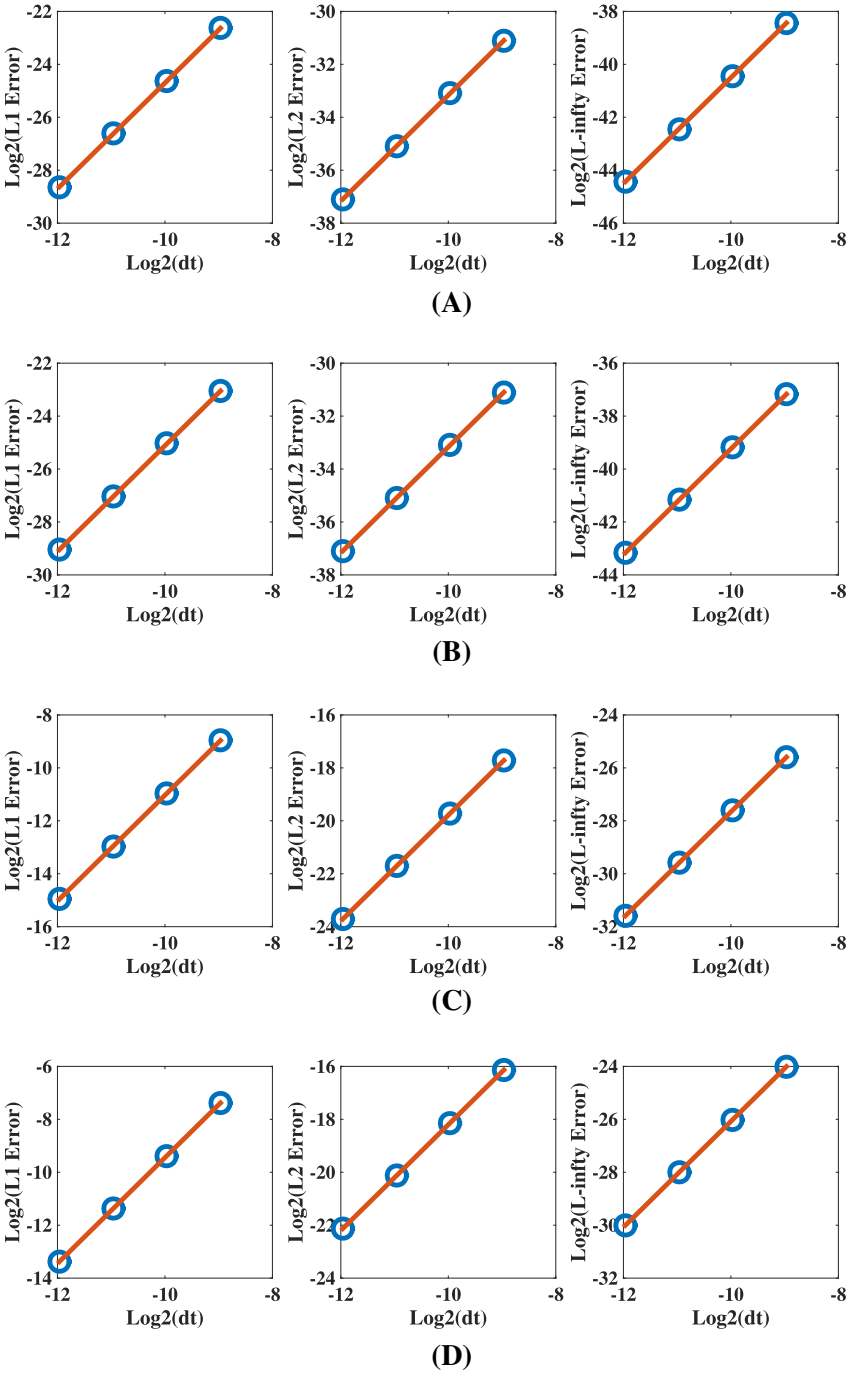

Fig. 3 Time step mesh refinement test for the 2nd order scheme. Here, we use spatial mesh size 512×512 and choose time step $\delta t = 2 \times 10^{-3}, 10^{-3}, 5 \times 10^{-4}, 2.5 \times 10^{-4}, 1.25 \times 10^{-4}$, respectively. The $\log_2(L_1, L_2, L_\infty$ norm of the error) for $\mathbf{v}$ and $\mathbf{Q}_{xx}, \mathbf{Q}_{xy}$ versus $\log_2(\delta t)$ are plotted. The slopes of the lines are all equal to 2. **a** Error of $\mathbf{v}_x$. **b** Error of $\mathbf{v}_y$. **c** Error of $\mathbf{Q}_{xx}$. **d** Error of $\mathbf{Q}_{xy}$

we finally obtain

$$\frac{1}{2}\|\mathbf{u}^{n+1}\|^2 + E^{n+1} + \frac{\delta t^2}{2}\|\nabla p^{n+1}\|^2 + \delta t\left(\eta\|\nabla\tilde{\mathbf{u}}^{n+1}\|^2 + M_1\|\mathbf{H}^{n+1}\|^2\right) \leq \frac{1}{2}\|\mathbf{u}^n\|^2 + E^n + \frac{\delta t^2}{2}\|\nabla p^n\|^2 + C^{n+1}\delta t^4. \tag{3.85}$$

□

Remark 3.3 We note that, in the momentum equation, a term Γ^n is added to cancel other terms generated from $u_\star^n$. This leads to the result that such a scheme is only "quasi"-energy stable, i.e. the energy decays modulo a quantity of order $O(\delta t^4)$.

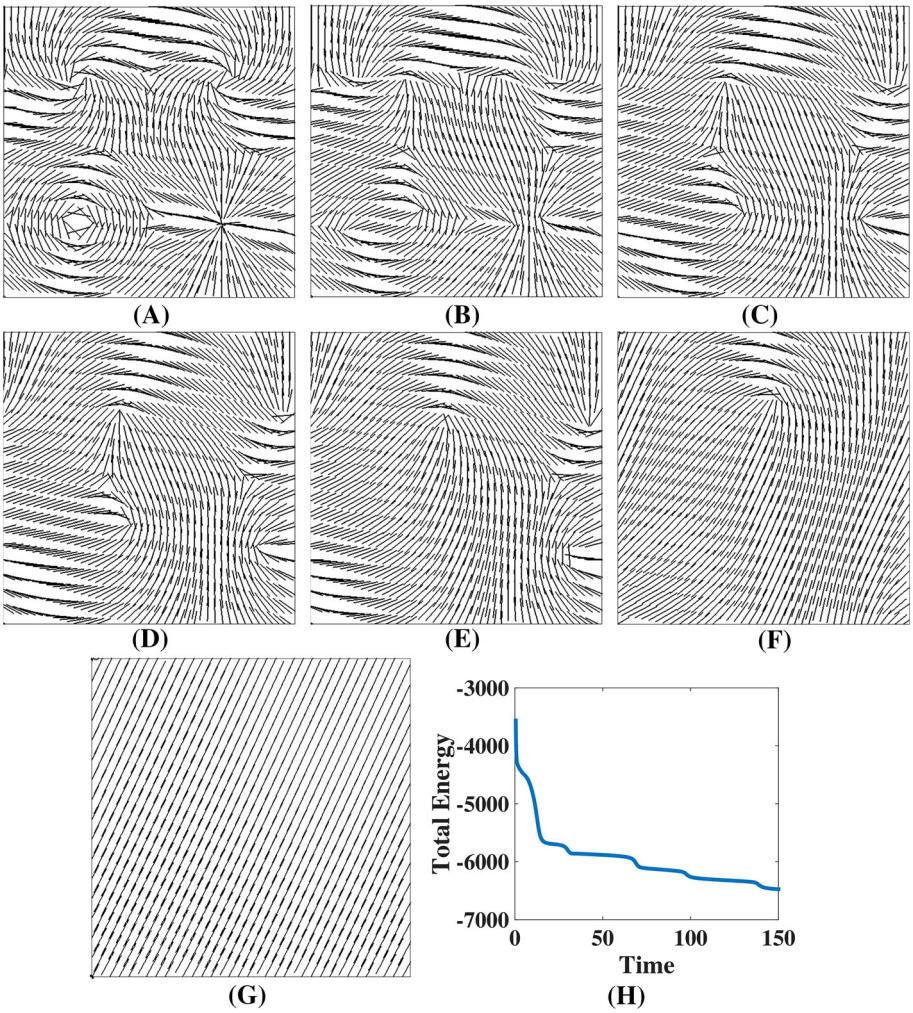

Fig. 4 Structure coarsening of defects in a channel flow. This figure shows coarsening dynamics of defects through splitting and annihilation. **a**–**g** the spatial structure at $t = 0, 10, 15, 25, 50, 100, 150$, respectively. In **h**, the total energy decay with time is shown. in the end ($t = 150$), the flow settles into a quiescent, homogeneous state without any defects. **a** $t = 0$. **b** $t = 10$. **c** $t = 15$. **d** $t = 25$. **e** $t = 50$. **f** $t = 100$. **g** $t = 150$. **h** discrte energy

4 Numerical Results

In this section, we first conduct the mesh refinement test in time to verify the convergence rate of the first order and the second order coupled scheme, respectively. Then, we will conduct several numerical simulations of liquid crystal flows in 2D channel geometries focusing on flow-induced defect dynamics. Here, we consider a lyotropic liquid crystal system with $\eta = 1$, $M_1 = 1$, $K = 0.001$, $\alpha = 1$, $N = 4$, and $a = 0.8$, respectively, which represents rod-like nematic liquid crystals. We use a rectangular computational domain, denoted by $[0, Lx] \times [0, Ly]$ in all the simulations below. In the following numerical study, we set $Lx = Ly = 1$, and we use periodic boundary condition in the x direction. In the y-direction, the boundary conditions are given as follows:

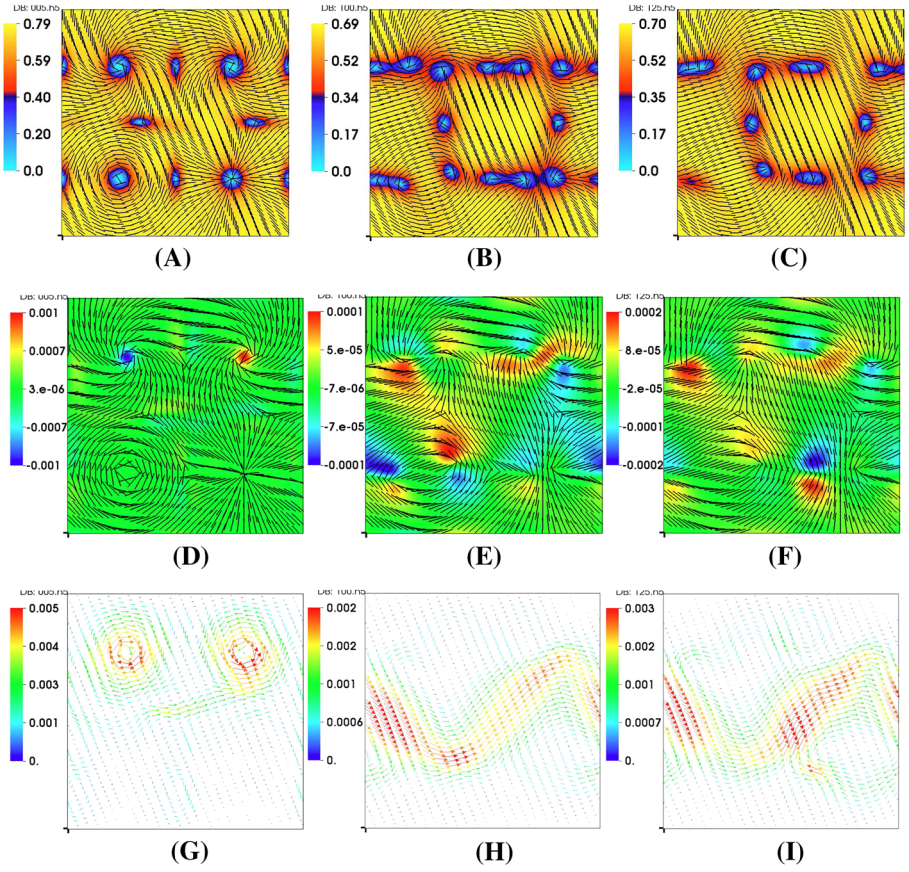

Fig. 5 Structure coarsening of defects in a channel flow. **a–c** show the difference between the largest and the second largest eigenvalues of $\mathbf{Q} + \mathbf{I}/3$ in the background pseudo-color map at time $t = 1, 10, 12.5$, respectively, in which defects are shown explicitly. Totally, 10 defects are initially identified, among which 4 are ± 1 defects and 6 are $\pm 1/2$ defects. The degree ± 1 defects split into degree $\pm 1/2$ defects and then $+1/2$ and $-1/2$ annihilate to reduce the number of defects in the domain eventually. **d–f** show the vorticity field as the background pseudo-color map at $t = 1, 10, 12.5$, respectively. **g–i** show the velocity field at time $t = 1, 10, 12.5$, respectively. **a** $t = 1$. **b** $t = 10$. **c** $t = 12.5$. **d** $t = 1$. **e** $t = 10$. **f** $t = 12.5$. **g** $t = 1$. h $t = 20$. **i** $t = 25$

$$\mathbf{u}|_{y=0,Ly} = 0, \quad \frac{\partial \mathbf{Q}}{\partial \mathbf{n}}|_{y=0,Ly} = 0. \tag{4.1}$$

The space is discretized by a second order finite difference method with central differencing. We use staggered grids, where $\mathbf{Q}$ and p are discretized at the cell center and $\mathbf{u}$ is discretized on cell edges. A schematic cartoon is shown in Fig. 1 to illustrate this idea.

4.1 Time Step Refinement Test

First, we conduct a mesh refinement test in time to confirm the order of the schemes. Notice that the schemes are coupled between the velocity field $\mathbf{v}$ and nematic field $\mathbf{Q}$. In the numerical implementation, we employ the extrapolation technique to decouple them. This should not affect any temporal accuracy. In order to have a high resolution in space to minimize the influence of the spatial error, we test the code in 2D spatial domain with the spatial mesh-size: 512×512 and time step $\delta t = 2 \times 10^{-3}, 10^{-3}, 5 \times 10^{-4}, 2.5 \times 10^{-4}$ and 1.25×10^{-4}, respectively. At $t = 1$, the numerical solutions are compared, where we calculate the error by treating the numerical result with its nearest finer time step as the approximation to the accurate solution. The errors for the first-order scheme in L_1, L_2 and L_∞ norm for $\mathbf{v}$ and $\mathbf{Q}$ are shown in Fig. 2, respectively. From the numerical tests, the first order scheme is shown at least first-order accurate in time. The second-order scheme is also implemented and the mesh

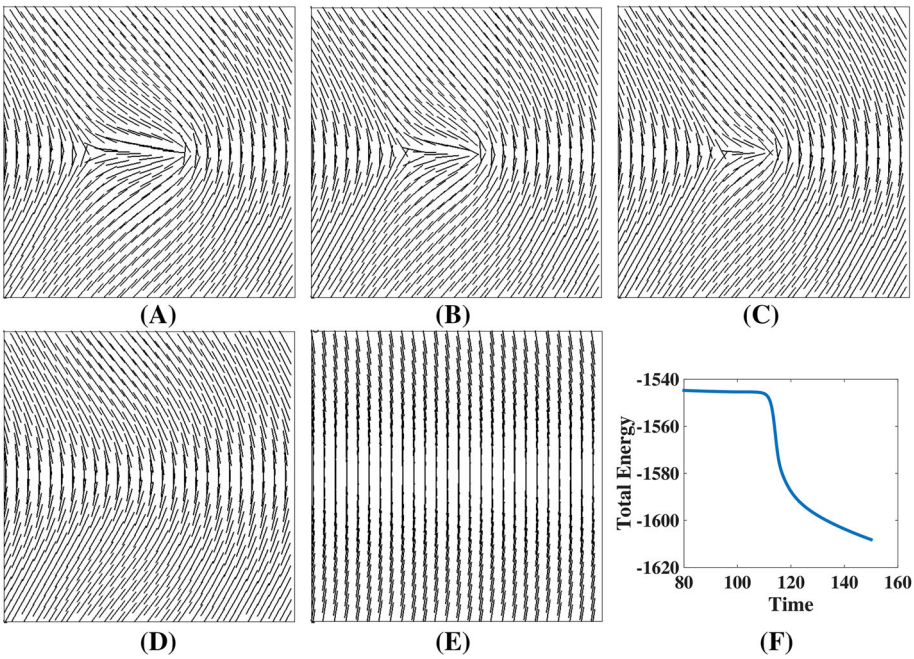

Fig. 6 Annihilation of a $+\frac{1}{2}$ defect and a $-\frac{1}{2}$ defect. This figure shows annihilation dynamics of two point defects with the opposite sign. **a–e** the nematic liquid crystal orientation on the xy plane at time $t = 80, 100, 110, 120, 150$, respectively; **f** the total energy decay with time t. **a** $t = 80$. **b** $t = 100$. **c** $t = 110$. **d** $t = 120$. **e** $t = 150$. **f** discrete energy

refinement test result is depicted in Fig. 3. From the numerical test, the numerical scheme is shown as second-order accurate.

We next apply this numerical scheme to study defect dynamics in liquid crystal flows during coarsening and defect annihilation.

4.2 Coarsening of Liquid Crystal Structures

In this simulation, we use the initial condition of a nematic liquid crystal phase on the xy plane, shown in Fig. 4a, where several defects are present. The coarsening dynamics of the orientational structure involving multiple defects are simulated. Several plots at various time steps are shown in Fig. 4a–g. We also plotted the discrete energy as a function of time in Fig. 4h, where we observe the energy decay with respect to time. Although there does not exist active hydrodynamic impact to the flow, its effect is coupled to liquid crystal orientational dynamics. This figure shows very interesting coarsening dynamics, where we observe $+1$ defects divide into two $+\frac{1}{2}$ defects (comparing Fig. 4a, b), as well as the annihilation of $-\frac{1}{2}$ and $+\frac{1}{2}$ defects, which can also be seen from the eigenvalues of $\mathbf{Q}$ on the xy plane, plotted in Fig. 5a–c. The velocity field and vorticity field are also shown in Fig. 5, from which, we observe relatively larger vorticity near the boundary of defects, as coarsening dynamics evolves. Initially there exists 10 defects, 4 degree ± 1 and 6 degree $\pm 1/2$. Eventually, the defects disappear due to annihilation. During the process, very complex defect dynamics are captured by the simulation.

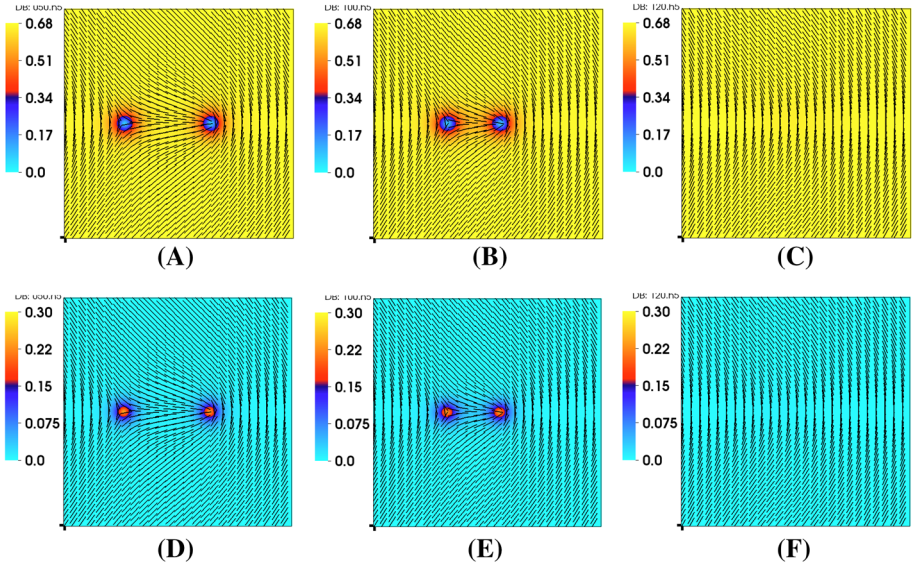

Fig. 7 Annihilation of a $+\frac{1}{2}$ defect and a $-\frac{1}{2}$ defect. This figure shows the differences between the three eigenvalues of $\mathbf{Q}+\mathbf{I}/3$, indicating the liquid crystal phase at the two point defects are biaxial. **a–c** The pseudo-color plot of the difference between the largest eigenvalue and the second largest eigenvalue of $\mathbf{Q}+\mathbf{I}/3$ is plotted at time $t = 50, 100, 120$, respectively. **d–f** The pseudo-color plot of the difference between the second largest eigenvalue and the smallest eigenvalue of $\mathbf{Q}+\mathbf{I}/3$ is plotted at time $t = 50, 100, 120$, respectively. Biaxiality of the liquid crystal system near the defects is shown in **d–f**. **a** $t = 50$. **b** $t = 100$. **c** $t = 120$. **d** $t = 50$. **e** $t = 100$. **f** $t = 120$

4.3 Annihilation and Repulsions of a Single Defect Pair

To better understand coarsening dynamics involving point defects, we conducted two more simulations, where annihilation of a $+\frac{1}{2}$ and $-\frac{1}{2}$ defects and the repulsion of two $+\frac{1}{2}$ defects are shown in Figs. 6 and 8, respectively. In both cases, we see decay of discrete energies with time (see Figs. 6f and 8f), which demonstrates the robustness of our energy-stable schemes. In particular, we have plotted the time series of the difference between the largest eigenvalue and the second largest one of $\mathbf{Q} + \mathbf{I}/3$ in Fig. 7a–c and the difference between the second largest eigenvalue and the smallest one in Fig. 7d–f, respectively. It demonstrates that the liquid crystal at the point defects are in fact biaxial [18] (as we have three distinct eigenvalues of $\mathbf{Q} + \mathbf{I}/3$ in the neighborhood of the point defects) and the liquid

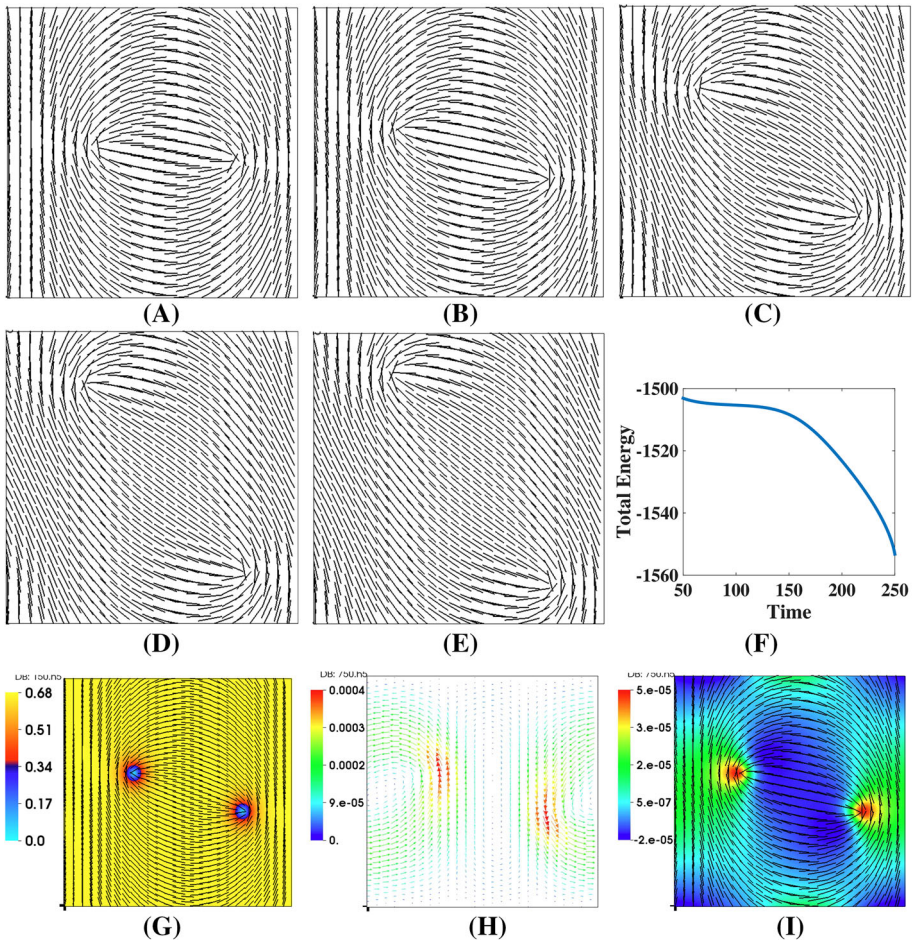

Fig. 8 Repulsion of two $+\frac{1}{2}$ point defects. This figure shows repulsion dynamics of two $+\frac{1}{2}$ point defects. **a–e** nematic liquid crystal orientation on the XY plane at time $t = 0, 50, 100, 150, 200, 250$, respectively. **f** the energy decay with time. **g** pseudo-color plot of the difference between the largest and the second largest eigenvalue of $\mathbf{Q}+\mathbf{I}/3$ is plotted. **h** The velocity field at $t = 150$ is shown; **i** The vorticity component at $t = 150$ is shown. **a** $t = 50$. **b** $t = 100$. **c** $t = 150$. **d** $t = 200$. **e** $t = 250$. **f** discrete energy. **g** $t = 150$. **h** $t = 150$. **i** $t = 150$

crystal is uniaxial elsewhere (as the second largest eigenvalue and the smallest eigenvalue are equal).

5 Conclusion

In this paper, we have developed several semi-discrete energy stable schemes for the Q-tensor based hydrodynamic model of nematic liquid crystals, which can be used to study flowing behavior of nematic liquid crystals in various geometries. These include both a first order and a second order scheme, together with a first-order decoupled approximation. The new schemes lay a solid foundation for pursuing further development of energy stable, efficient numerical methods for solving hydrodynamic models of complex fluids that obey energy dissipation laws. The schemes are then used to study defect dynamics during coarsening of nematic liquid crystal orientational structures and pair interaction between point defects. The numerical schemes are shown to be effective in solving the Q-tensor based hydrodynamic model of liquid crystals. The methodology developed here also provides a paradigm for developing energy-stable schemes for more general hydrodynamic models of complex fluids, which obey an energy dissipation law.

Acknowledgments Jia Zhao and Qi Wang are partially supported by NSF-DMS-1200487 and NSF-DMS-1517347, NIH-2R01GM078994-05A1, AFOSR-FA9550-12-1-0178, and an SC EPSCOR/IDEA award. In addition, Jia Zhao is also supported by a Dissertation Fellowship from the Provost Office of USC.

References

1. Beris, A.N., Edwards, B.: Thermodynamics of Flowing Systems. Oxford Science Publications, New York (1994)
2. Blow, M.L., Thampi, S.P., Yeomans, J.M.: Biphasic lyotropic active nematics. Phys. Rev. Lett. **113**, 248303 (2014)
3. Boyer, F., Lapuerta, C.: Study of a three component Cahn–Hilliard flow model. ESAIM Math. Model. Numer. Anal. **40**(4), 653–687 (2006)
4. de Gennes, P.G., Prost, J.: The Physics of Liquid Crystals. Oxford University Press, Oxford (1993)
5. Denniston, C., Orlandini, E., Yeomans, J.M.: Lattice boltzmann simulations of liquid crystal hydrodynamics. Phys. Rev. E **63**(5), 056702 (2001)
6. Doi, M., Edwards, S.F.: The Theory of Polymer Dynamics. Oxford Science Publication, New York (1986)
7. Fan, J., Ozawa, T.: Regularity criteria for a coupled Navier–Stokes and q-tensor system. Int. J. Anal. **2013**, 718173 (2013)
8. Forest, M.G., Wang, Q.: Hydrodynamic theories for mixtures of polymers and rodlike liquid crystalline polymers. Phys. Rev. E **72**, 041805 (2005)
9. Forest, M.G., Wang, Q., Zhou, H.: Homogeneous biaxial patterns and director instabilities of liquid crystal polymers in axial and planar elongation. Phys. Fluids **12**, 490–498 (2000)
10. Guillenn-Gonzalez, F., Rodriguez-Bellido, M.A.: Weak time regularity and uniqueness for a q-tensor model. SIAM J. Math. Anal. **46**(5), 3540–3567 (2014)
11. Guillenn-Gonzalez, F., Rodriguez-Bellido, M.A.: Weak solutions for an initial boundary q tensor problem related to liquid crystals. Nonlinear Anal. **112**, 84–104 (2015)
12. Han, D., Wang, X.: A second order in time uniquely solvable unconditionally stable numerical schemes for Cahn–Hilliard–Navier–Stokes equation. J. Comput. Phys. **290**(1), 139–156 (2015)
13. Leslie, F.M.: The theory of flow phenomena in liquid crystals. Adv. Liq. Cryst. **4**, 1–81 (1979)
14. Longa, L., Trebin, H.R.: Spontaneous polarization in chiral biaxial liquid crystals. Phys. Rev. A **42**(6), 3453 (1990)
15. MacDonald, C.S., Mackenzie, J.A., Ramage, A.: Efficient moving mesh method for q-tensor models of nematic liquid crystals. SIAM J. Sci. Comput. **37**(2), 215–238 (2015)
16. Marenduzzo, D., Orlandini, E., Yeomans, J.M.: Hydrodynamics and rheology of active liquid crystals a numerical investigation. Phys. Rev. Lett. **98**, 118102 (2007)

17. Paicu, M., Zarnescu, A.: Energy dissipaiton and regularity for a coupled Navier–Stokes and q-tensor system. Arch. Ration. Mech. Anal. **203**, 45–67 (2012)
18. Schopohl, N., Sluckin, T.J.: Defect core structure in nematic liquid crystals. Phys. Rev. Lett. **59**(22), 2582 (1987)
19. Shen, J., Wang, C., Wang, S., Wang, X.: Second-order convex splitting schemes for gradient flows with Ehrlich–Schwoebel type energy: application to thin film epitaxy. SIAM J. Numer. Anal. **50**(1), 105–125 (2012)
20. Shen, J., Yang, X.: Numerical approximation of Allen–Cahn and Cahn–Hilliard equations. Discrete Contin. Dyn. Syst. Ser. B **28**(4), 1669–1691 (2010)
21. Shen, J., Yang, X.: Decoupled energy stable schems for phase field models of two phase complex fluids. SIAM J. Sci. Comput. **36**(1), 122–145 (2014)
22. Sonnet, A.M., Maffettone, P.L., Virga, E.G.: Continuum theory for nematic liquid crystals with tensorial order. J. Non-Newton. Fluid Mech. **119**, 51–59 (2004)
23. Sulaiman, N., Marenduzzo, D., Yeomans, J.M.: Lattice boltzmann algorithm to simulate isotropic–nematic emulsions. Phys. Rev. E **74**, 041708 (2006)
24. Temam, R.: Navier–Stokes Equations: Theory and Numerical Analysis. American Mathematical Society, Providence (2001)
25. Tsuji, T., Rey, A.D.: Effect of long range order on sheared liquid crystalline materials, part I: compatability between tumbiling and behavior and fixed anchoring. J. Non-Newton. Fluid Mech. **73**, 127–152 (1997)
26. Wang, C., Wise, S.M.: An energy stable and convergent finite-difference scheme for the modified phase field crystal equation. SIAM J. Numer. Anal. **49**, 945–969 (2011)
27. Wang, Q.: Biaxial steady states and their stability in shear flows of liquid crystal polymers. J. Rheol. **41**, 943–970 (1997)
28. Wang, Q.: A hydrodynamic theory of nematic liquid crystalline polymers of different configurations. J. Chem. Phys. **116**, 9120–9136 (2002)
29. Wise, S.M., Wang, C., Lowengrub, J.S.: An energy-stable and convergent finite-difference scheme for the phase field crystal equation. SIAM J. Numer. Anal. **47**(3), 2269–2288 (2009)
30. Yang, X.: Error analysis of stabilized semi-implicit method of Allen–Cahn equation. Discrete Contin. Dyn. Syst. Ser. B **11**, 1057–1070 (2009)
31. Yang, X., Feng, J.J., Liu, C., Shen, J.: Numerical simulations of jet pinching-off and drop formation using an energetic variational phase-field method. J. Comput. Phys. **218**, 417–428 (2006)
32. Yang, X., Forest, M.G., Mullins, W., Wang, Q.: 2-D lid-driven cavity flow of nematic polymers: an unsteady sea of defects. Soft Matter **6**, 1138–1156 (2010)
33. Yang, X., Forest, M.G., Wang, Q.: Near equilibrium dynamics and one-dimensional spatial–temporal structures of polar active liquid crystals. Chin. Phys. B **23**(11), 118701 (2014)
34. Yang, X., Wang, Q.: Capillary instability of axisymmetric active liquid crystal jets. Soft Matter **10**(35), 6758–6776 (2014)